

A Near-IR Spectroscopic Survey of FU Orionis Objects

Michael S. Connelley^{1,2} and Bo Reipurth¹

*University of Hawaii at Manoa, Institute for Astronomy,
640 North Aohoku Place, Hilo, HI 96720, USA*

ABSTRACT

We have conducted a homogenous near-IR spectroscopic survey of 33 objects with varying degrees of similarity to FU Orionis.

Common spectroscopic features that are characteristic of the three classical FUors FU Ori, V1057 Cyg, and V1515 Cyg are: strong CO absorption, weak metal absorption, strong water bands, low gravity, strong blue shifted He I absorption, and few (if any) emission lines. Based on these criteria, we classify the 33 objects as either bona fide FUors (eruption observed), FUor-like objects (eruption not observed), or peculiar objects with some FUor-like characteristics, and present a spectral atlas of 14 bona-fide FUors, 10 FUor-like objects, and 9 peculiar objects. All objects that we classify as FUors or FUor-like have very similar near-IR spectra. We use this spectral similarity to determine the extinction to each source, and correlate the extinction to the depth of the 3 μm ice band. All bona fide FUors still today maintain the spectrum of a FUor, despite the eruption occurring up to 80 years ago. Most FUors and FUor-like objects occupy a unique space on a plot of Na+Ca vs. CO equivalent widths, whereas the peculiar objects tend to be found mostly elsewhere. Since most FUors show a reflection nebula, we also present an atlas of K-band images of each target. We found that the near-IR spectra of FUors and young brown dwarfs can be extremely similar, a distinguishing feature being the Paschen β absorption in the spectra of FUors. Although V1647 Ori, AR 6a, and V346 Normae had been previously classified as candidate FUors, we classify them as peculiar objects with some FUor-like properties since their spectra now differ significantly from bona fide FUors. We confirm two new FUor-like objects that were initially identified as candidates based on their near-IR morphology.

²Staff Astronomer at the Infrared Telescope Facility, which is operated by the University of Hawaii under contract NNH14CK55B with the National Aeronautics and Space Administration.

Subject headings: stars: formation – stars: protostars – stars: pre-main sequence
– infrared: stars – techniques: spectroscopic

1. Introduction

The major eruption of FU Ori in 1936 marked an important point in the study of early stellar evolution, although nobody realized it at the time (Wachmann 1954). It was Herbig (1966) who argued that FU Ori represented some phenomenon of stellar youth. In 1969 another very similar eruption took place in V1057 Cyg (Welin 1971a,b) indicating that FU Ori was not a pathological case but a member of a new class of objects, for which Ambartsumian (1971) coined the term FUor. In a classical study, Herbig (1977) presented detailed optical spectra of three FUors, showing that they all possessed cool supergiant spectra, with the peculiarity that the spectra become increasingly late when observed at longer wavelengths, and displaying a strong lithium line. Of special importance, Herbig demonstrated that V1057 Cyg prior to its eruption was a T Tauri star. Reviews about FUors include Reipurth (1990), Hartmann & Kenyon (1996), Reipurth & Aspin (2010), and Audard et al. (2014). Historical details about Herbig’s work on FUors are discussed in Reipurth (2016).

Hartmann & Kenyon (1985) suggested that the FUor phenomenon represents a short-lived major increase in disk accretion, and in a series of papers they were able to explain many of the observed features of FUors with this model. The spectral energy distributions of FUors are reproduced well by modern disk models with accretion rates of about $10^{-5} M_{\odot} \text{ yr}^{-1}$ (e.g., Zhu et al. 2008). Accretion rates of FUors are thus several orders of magnitude larger than for typical T Tauri stars, and the FUor phenomenon may therefore play a significant role in the mass assembly of young stars, and may also explain the significant luminosity spread observed among embedded stars (e.g., Baraffe et al. 2012).

Various ideas have been proposed to explain the triggering of FUor outbursts. The first is a throttle mechanism that controls the passage of gas through the inner disk (e.g., Zhu et al. 2009). The disk may receive gas from an infalling envelope at a different rate than it transfers through the disk, sometimes causing material to pile up, which may later be released and causing an eruption. The second also deals with a disk that receives gas from an infalling envelope and assumes that if the accretion rate through a disk increases, and thus the disk temperature, then the opacity of the gas may rise so fast that heat becomes trapped in the disk and a runaway situation develops during which the inner disk may be emptied out (e.g., Bell & Lin 1994, Armitage et al. 2001). The third mechanism proposes that a companion in an eccentric orbit perturbs the disk at periastron (Bonnell & Bastien

1992, Reipurth & Aspin 2004a). Perturbations by a planet (Clarke et al. 2005) or with another member of a dense cluster (Pfalzner 2008) have also been considered. Finally, the fourth idea assumes accretion of a large body, like a planet (Larson 1980) or a large ‘gas blob’ in a circumstellar disk (Vorobyov & Basu 2015).

George Herbig and Peter Petrov proposed an alternative to the disk model in a series of papers (Herbig et al. 2003, Petrov & Herbig 1992, 2008), and concluded that the *optical* spectra are caused by a rapidly rotating bloated star near the edge of instability, as originally proposed by Larson (1980). Interestingly, the bloated star scenario and the disk accretion concept are not mutually exclusive: Recent calculations of episodic accretion onto low-mass protostars suggest that, for sufficiently high accretion rates, the central star may expand significantly, thus increasing its luminosity far beyond the expectation based on its mass and age (e.g., Hosokawa et al. 2011, Baraffe et al. 2012). Thus, optical spectra may primarily refer to the central object – extended due to rotation near breakup speed (Larson 1980) – while infrared observations are dominated by disk emission further out.

No FUor has been observed to undergo more than one eruption (although the peculiar object V1647 Ori, which has certain FUor characteristics, had a prior outburst), but through a statistical analysis Herbig (1977) showed that the phenomenon must be recurrent with an outburst rate of roughly 10^{-4} per year per star in a star forming region. Subsequent studies have supported this conclusion, albeit with somewhat different outburst rates (e.g., Hartmann & Kenyon 1996, Hillenbrand & Findeisen 2015). Currently only about two dozen FUors and FUor-like objects are known, and better statistics will emerge as ongoing wide field surveys identify new cases.

Spectroscopically FUors share certain broad characteristics: the significant P Cygni profiles at specific lines, the gradually cooler spectra at longer wavelengths, and the low-gravity spectral appearance. But photometrically FUors form a rather heterogeneous group, with a significant difference in rise-times for different objects, ranging from approximately a year for FU Ori and V1057 Cyg to more than 15 years for V1515 Cyg, and also major differences in decay times: V1057 Cyg has already faded to only about 2 magnitudes brighter than its original brightness, whereas for example V883 Ori and BBW 76 are still bright more than a century after their presumed eruptions. On much shorter timescales, EXors can attain almost the same amplitudes as FUors, but they decay on timescales of a year and typically have strong emission-line spectra (Herbig 2007, 2008). And some eruptive variables defy classification (e.g., Herczeg et al. 2016). As more and more young objects are found to erupt (e.g., Contreras Peña et al. 2016), an ever wider range of photometric behaviors may well emerge. It thus appears likely that spectroscopic criteria will form a firmer basis for classification of eruptive variables. And since an increasing number of eruptions are found

among embedded objects, infrared spectroscopy may emerge as a critical tool to distinguish between different categories of objects.

In this paper, we present an atlas of near-infrared spectra of all currently accepted or probable FUors and FUor-like objects, as well as of a few eruptive variables which are sometimes suggested as FUors. We attempt to identify common spectroscopic characteristics of the FUors, which may prove useful for future classifications.

2. Observations

Our observations were carried out with the 3.0 m NASA Infrared Telescope Facility (IRTF) on Maunakea, Hawaii with the recently upgraded SpeX instrument in the short cross-dispersed mode, which covers $0.7 \mu\text{m}$ to $2.5 \mu\text{m}$ in each exposure (Rayner et al. 2003). We used the $0''.5$ wide slit, which gives a resolving power of $R=1200$. Stars were nodded along the slit, with two exposures taken at each nod position. The total exposure time was driven by our goal to get a high S/N spectrum for each target on each night. The individual exposure times were limited to three minutes to ensure that the telluric emission lines would cancel when consecutive images taken at alternate nod positions were differenced. An A0 telluric standard star was observed after at least every other science target for telluric correction, usually within 0.1 air masses of the target. Our observing log is shown in Table 1.

An argon lamp was observed for wavelength calibration and a quartz lamp for flat fielding. An arc/flat calibration set was observed for each target/standard pair. The SpeX data were flat fielded, extracted, and wavelength calibrated using *Spextool* (Cushing et al. 2004). After extraction and wavelength calibration, the individual extracted spectra were co-added with *xcombspec*. *Xtellcor* was then used to construct a telluric correction model using the observed A0 standard, after which the observed spectrum of the target was divided by the telluric model. Finally, *xmergeorders* was used to combine the spectra in the separate orders into one continuous spectrum. However, wavelength regions where the J, H and K orders overlap are noisy due to atmospheric opacity, and thus the scaling of the orders can adversely affect the flux ratio of lines in different orders. As such, we did not scale the orders prior to merging so as to best preserve the line flux ratios, which is particularly important in determining the extinction. These codes are all IDL routines written by Cushing et al. (2004) to reduce SpeX data. Spectral line flux, equivalent width, and FWHM were measured using the SPLLOT routine in IRAF.

When the observing conditions were photometric, we took K-band images for flux calibration using the SpeX guider camera. For these imaging data, the telescope was dithered

using a nine point $10''$ pattern to allow us to make "sky flats" from the data. A dark frame was made by averaging together 10 individual dark frames of the same exposure time as the science data. This dark was then subtracted from each target frame. Sky flats were made by scaling each dark subtracted image to have the same median value, then averaging them together using a min-max rejection. The resulting sky flat was then normalized using the median value of the pixel counts. Each dark subtracted (but not scaled) target frame was divided by this normalized sky flat. The median sky value for each frame was subtracted from each frame to set the average background counts in each frame to 0 to account for changes in the brightness of the sky. The images were then aligned and averaged together using an average sigma clipping rejection. Standard stars that have been observed by UKIRT through the MKO filter set (Simons & Tokunaga 2002, Tokunaga & Simons 2002) were selected from the UKIRT faint standard star list, and were observed for photometric calibration.

Table 2 lists details of the 33 objects discussed in this paper.

3. What is a FUor?

Attention was originally drawn to FU Ori because of its major and rapid brightening. Similarly, the next two FUors to be recognized, V1057 Cyg and V1515 Cyg, were discovered because of their brightenings, albeit not as rapid as that of FU Ori. In his pioneering study, Herbig (1977) identified the optical spectroscopic characteristics of these three objects, which are now universally accepted as 'classical' FUors.

Since then a wealth of objects have been classified as FUors, with justifications that range from solid to at best tenuous. It is noteworthy that there are now many objects that have been classified as FUors based on their spectra rather than on the basis of an observed outburst. Evidently this easily leads to a rather heterogeneous group of objects.

While Herbig's analysis was based on optical high-resolution spectra, many of the more recent discoveries of FUors are sufficiently embedded that they can only be observed in the infrared. We therefore attempt to define here the *near-infrared* spectral characteristics of FUors, based on the three classical FUors discussed in Herbig (1977). In the following we examine the near-infrared spectra of FU Ori, V1057 Cyg, and V1515 Cyg.

3.1. Near-IR Spectral Characteristics of FU Ori, V1057 Cyg, and V1515 Cyg

Figure 1 shows the near-infrared spectra in the J, H, and K bands of the three classical FUors FU Ori, V1515 Cyg, and V1057 Cyg. All three stars have only modest extinction

(see Appendix A and Table 2) and their spectra in Figure 1 are not corrected for this minor reddening. In the following we describe the spectral characteristics that these three stars have in common.

- **CO.** Strong absorption at the CO bands, starting at $2.29 \mu\text{m}$, is perhaps the most visible characteristic of the three FUors, and in the past it has been used as a spectroscopic characteristic to identify candidate FUors whose eruptions were not observed. However, we caution that *strong CO absorption is necessary but alone is not sufficient* to characterize a YSO as a FUor. Several other YSOs have spectra that show strong CO absorption (e.g., IRAS 06393+0913), but lack other important spectroscopic characteristics of FUors (Connelley & Greene 2010). The equivalent width of the bluest CO band of FU Ori is slightly greater than for a late-M dwarf, but less than a late-M giant (per the SpeX library, Rayner et al. 2009).

It is noticeable that our spectrum of V1057 Cyg does not show the same pronounced CO absorption as the other two FUors. The first near-infrared spectra of FU Ori and V1057 Cyg were obtained 40 years ago in 1977 by Mould et al. (1978), only eight years after the eruption of V1057 Cyg. Visual comparison of the CO bands in these spectra of FU Ori and V1057 Cyg show them to be of equal strength (see Fig. 1 of Mould et al. 1978), as they also appear to be in the spectra obtained in 1986 by Hartmann & Kenyon (1987). Their much weakened appearance in our new spectra of V1057 Cyg is thus a more recent development. There seem to be two possible explanations. First, we note that V1057 Cyg has faded considerably since its eruption, more than any other known FUor, and it is now about 2/3 of the way down to its pre-outburst range (e.g., Kopatskaya et al. 2013). Since most of the light from a FUor emanates from the disk, the star (or central bloated object) may therefore now contribute a larger fraction of the light from V1057 Cyg. Second, we speculate that the disk could have undergone a structural change, somehow losing the outer disk regions which mainly contribute the CO bands (see Figure 5 of Calvet et al. 1991), possibly as the result of dynamical interactions with a binary companion.

- **Water vapor bands.** The continuum profiles of the three classical FUors superficially appear similar to a mid-M type star. Strong water vapor bands on each end of the H-band window shape the H-band continuum into a characteristic triangular shape. All three classical FUors have a 'peaky' or 'triangular' H-band continuum that is often interpreted as a signature of low gravity in young stars, in contrast to the more rounded appearance seen in evolved stars. There are also strong breaks in the continuum at $1.33 \mu\text{m}$ and $2.29 \mu\text{m}$ due to the onset of water vapor absorption.

- **Other molecular bands.** The J-band spectra show rather wide absorption from Vanadium oxide bands around $1.05 \mu\text{m}$ and $1.19 \mu\text{m}$. These bands are highly sensitive to gravity, and are not visible in M-dwarfs, but begin to appear at spectral type M7 for

higher luminosity stars (e.g., Rayner et al. 2009). The TiO bands that so dominate the red end of optical spectra of late-type stars reach slightly into the J-band, and weak bands are discernible in V1515 Cyg at 0.88, 0.92, and 1.11 μm , but only at 1.11 μm for the other two sources.

- **Hydrogen lines.** The Paschen- α , β , γ , δ lines are pronounced absorption lines in the J and H-bands. The Brackett series of lines are generally not observed. Brackett γ , a line frequently observed in young stars and often associated with mass accretion, is very weakly seen at K-band with a possible P Cygni profile.

- **Absence of emission lines.** In contrast to other young erupting stars like the EXors, FUors tend to have few, if any, emission lines. As in the optical wavelength range, the three classical FUors show emission in the J, H, K bands exclusively as strong P Cygni profiles, notably at the Ca II triplet at 0.850, 0.854, and 0.866 μm . In particular, we note that Pa β and H $_2$ are *not* seen in emission, while Br γ appears very weak with a possible P Cygni profile.

- **Metallic lines.** Absorption from Na (2.208 μm) and Ca (2.256 μm) are weakly observed in the three FUor spectra. The EW of these lines is less than half that of a late-M giant. For 9 photospheric lines from several species, the median of the ratio of EWs measured in the spectrum of FU Ori compared to an M7 giant is 0.55.

- **Helium I.** The He I line at 1.083 μm is a pronounced absorption line in the spectra of all three FUors. The blue edge of the line has a velocity of -300 km s^{-1} , -400 km s^{-1} , and -400 km s^{-1} for FU Ori, V1515 Cygni, and V1057 Cygni, respectively.

- **Gradual change of spectral type with wavelength.** We note that the main optical spectroscopic peculiarity recognized by Herbig (1977) in these three stars, namely the gradual change towards later spectral types at longer wavelengths, is not obvious from the J to the K band, presumably due to the rather low spectral resolution. But the overall spectral type of the three stars is late M, which is much later than the spectral types derived by Herbig in the optical range.

In summary, each of the above spectral characteristics of the three classical FUors is seen in other stars. But if one focuses only on young stars, the *combination* of these spectral characteristics is unique to the FUors. Hence the first task when faced with a potential new FUor is to establish – or at least make plausible – the youth of an erupting object. While lithium offers one such assurance in optical spectra, no similar line is available in the near-infrared. Hence, for embedded objects for which lithium is unobservable, an infrared excess, an association with a reflection nebula, or at least association with a star forming

region or molecular cloud, are important additional criteria.¹

In consequence, attaching the label of FUor or FUor-like to an object will necessarily be done with varying degrees of confidence, depending on how many of the above characteristics are observed. In many cases, the firm classification of an object as a FUor or FUor-like object will require the gradual accumulation over time of the necessary information.

4. Comments on Individual Objects

In the following we evaluate the spectra and the photometric histories together with other pertinent information for each of 33 objects, all of which have at some point been suggested as FUors. Table 2 lists basic information about each of the 33 objects as well as our evaluation of their classification. Table 3 presents the basis for our classification of each object.

Not all of these objects have been observed to undergo an eruption. We therefore divide the 33 objects into three categories: (1) bona fide FUors with spectra displaying the near-infrared spectral characteristics recognized in Section 3 and with witnessed eruptions, (2) FUor-like objects that similarly have spectra like FUors but for which an eruption was not witnessed, and (3) objects that have (or have had) some spectral similarities to FUors, but enough differences that a FUor classification is not warranted. In Appendix C, we additionally describe a few objects that in the past have been erroneously classified as FUors.

4.1. Bona Fide FUors

We here discuss 14 objects that have been observed to erupt and whose spectra are very similar to those of the classical FUors discussed in Section 3, and which we therefore deem to be bona fide FUors. Their near-infrared spectra are shown in the spectral atlas in Figure 2. Since some of these 14 objects suffer considerable extinction, we have dereddened their spectra and plotted them next to each other in Figure 3, which facilitates a direct comparison of their spectra with those of the three classical FUors. The He I absorption line and the CO absorption bands are important characteristics of FUors, and these features are shown in detail in Figures 4 and 5, respectively.

¹A similar condition was required by Herbig (1960) when he defined what is now known as Herbig Ae/Be stars. When later researchers abandoned the requirement of a reflection nebula, the catalogs of Herbig Ae/Be stars became polluted with many stars that are not young.

RNO 1b: This object, also known as V710 Cas, was identified as a new FUor by Staude & Neckel (1991), who noticed that it had brightened by at least 3 magnitudes between 1978 and 1990. Their optical spectrum is consistent with a FUor, showing $H\alpha$ and Li in absorption, with a blueshifted absorption trough at $H\alpha$. The near-IR spectrum in Greene & Lada (1996) and the one shown here show strong CO absorption, 'triangular' H band, and a clear break in the continuum at $1.33 \mu\text{m}$ from water vapor.

V582 Aurigae: The amateur astronomer Anton Khruslov discovered the eruption of this star (Samus 2009). It is located in the L1516 cloud at a distance of 1.3 kpc (Kun et al. 2017). Semkov et al. (2013) found that the eruption happened between late 1984 and early 1985 based on archival photographic plates, and showed that the optical spectrum displays typical strong P Cyg profiles at $H\alpha$ and the Sodium doublet. Our spectrum is the first IR spectrum of this target, and it shows the typical FUor characteristics: CO absorption, a 'triangular' H band, and a clear water vapor break in the continuum at $1.33 \mu\text{m}$.

V883 Orionis: This source is optically very faint but at infrared wavelengths it is one of the most luminous sources in the L1641 cloud in Orion. The source was suggested as a FUor by Strom & Strom (1993) based on an optical spectrum of its reflection nebula which shows a blueshifted absorption profile of $H\alpha$. The K-band spectrum presented in Reipurth & Aspin (1997) showing strong CO absorption and a featureless continuum is consistent with our spectrum, which additionally shows the characteristic triangular H-band continuum, a strong break at $1.33 \mu\text{m}$, VO bands, and no emission lines. The source is associated with the little HH object HH 183, and illuminates the small optical reflection nebula IC 430. The IC 430 nebula was significantly larger and brighter in 1888 when – as discussed by Strom & Strom (1993) – Pickering (1890) photographed the region. This is reminiscent of the bright reflection nebulae that appeared when V1057 Cyg and V1647 Ori erupted, and we accept the bright state of IC 430 around 1888 as evidence of a prior eruption, and accordingly classify the object as a bona fide FUor. Cieza et al. (2016) used ALMA observations to determine a dynamical mass of $1.3 \pm 0.1 M_{\odot}$ for V883 Ori, and found evidence that the water-line was moved outwards in the disk during the eruption, although Schoonenberg et al. (2017) offer a different interpretation.

V2775 Orionis: The outburst of this object occurred between March 2007 and November 2008, with an increase in brightness of 3.8 magnitudes at K-band, as documented by Caratti o Garatti et al. (2011). Their near-IR spectrum shows several of the features that characterize FUor spectra: strong water and CO absorption, a 'triangular' H-band continuum, VO bands and no emission lines. Fischer et al. (2012) observed He I absorption blue-shifted by $\sim 300 \text{ km s}^{-1}$. Whereas our spectrum also shows He I absorption, it is much weaker and is centered at the rest wavelength. This object has only been detected at infrared

wavelengths, and we argue in Appendix A that this object is on the back side of its cloud.

FU Orionis: The eruption of FU Ori was observed in 1936 (Wachmann 1954, Herbig 1966). The light curve shows a rapid brightening by ~ 5.5 magnitudes over 8 months, followed by a slow decline of $\sim 1/2$ magnitude over the next 40 years with small-scale faster variability (Herbig 1977). Wang et al. (2004) noted a highly reddened faint companion $0''.5$ south of FU Ori, which was demonstrated to be a young star by Reipurth & Aspin (2004a), and Beck & Aspin (2012) and Pueyo et al. (2012) determined that this companion is the more massive component of the FU Ori binary. FU Ori is the prototype of the FUors, and since it suffers very little extinction we use its spectrum as the reference for all other potential FUors.

V900 Monocerotis: The outburst of this target was first noticed in 2009 by Thommes et al. (2011). Optical and IR spectra taken by Reipurth et al. (2012) confirmed several FUor-like spectral features. The object is a partly embedded Class I object with a considerable extinction of about $A_V \sim 13$ magnitudes. Infrared photometry by Varricatt et al. (2017) suggests that the object is still brightening. Our spectrum of V900 Mon appears to be consistent with the spectrum in Reipurth et al. (2012) and displays all the FUor characteristics discussed in Sect. 3.1.

V960 Monocerotis: This object is also known as 2MASS J06593158-0405277. It is a recent FUor whose eruption was first noticed on Nov 3, 2014 by Maehara et al. (2014). The outburst happened between January and October 2014. Hackstein et al. (2015) presented the light-curve for this target back to Nov 2010, showing the target getting brighter in the R-band and I-band by ~ 2.6 magnitudes. After the outburst was discovered, Hackstein et al. (2015) found that the R-band brightness declined by ~ 0.5 magnitudes in the following 6 months while showing a low-amplitude 17-day oscillation, which they interpreted as evidence for a (unseen) companion. Kóspál et al. (2015) found V960 Mon to be associated with 8 likely T Tauri stars and an embedded Class 0 source. Jurdana-Sepic & Munari (2016) found no other eruptions in a historical light curve spanning from 1899 to 1989. Caratti o Garatti et al. (2015) imaged a faint companion at a $0''.2$ separation, and possibly another even closer companion. We observed it on Dec 22, 2014, very shortly after the eruption was announced, when the object was at $K=7.42$, whereas the 2MASS magnitude is $K=9.45$. The spectrum displays all the FUor characteristics.

V1515 Cygni: This object is located near the NGC 6914 region in Cygnus at an approximate distance of 1050 pc according to Racine (1968). It was first identified as a FUor by Herbig (1977), and the FUor classification was further supported by the observations presented by Kenyon et al. (1991). The light curve in Herbig (1977) shows a slow and gradual brightening over ~ 10 years, starting in about 1950, different from the very rapid rise of FU Orionis. Clarke et al. (2005) extend the light curve to 2003, showing a slow gradual

decline with ~ 0.3 magnitudes of short-term variability. Optical spectra taken around 1974 show a high luminosity G type star, with P Cygni profile at $H\alpha$, and strong lithium at 671 nm. The K-band spectrum presented by Reipurth & Aspin (1997) shows the strong CO absorption characteristic of FUors. Our spectrum is discussed in Sect. 3.1.

HBC 722: Also known as V2493 Cygni. A faint visible star erupted in July 2010 and brightened by $R \sim 4.2$ magnitudes in ~ 2 months (Semkov et al. 2010, 2012). It is associated with the small cluster around LkH α 188 that is located in the active star forming cloud L935 in the North America Nebula at a distance of 550 pc (e.g., Armond et al. 2011). Shortly after the outburst was noticed, the optical spectrum of this object was observed to be similar to FUors (e.g., Munari et al. 2010). Importantly, a pre-outburst optical spectrum was fortuitously recorded and found to be consistent with a classical T Tauri star showing hydrogen emission with a K7-M0 spectral type (Cohen & Kuhl 1979, Miller et al. 2011). Despite undergoing an outburst of accretion, the non-detection of this source in the sub-millimeter by SMA puts an upper limit on the total circumstellar material at $0.02 M_{\odot}$ (Dunham et al. 2012). After the initial eruption, HBC 722 faded slightly, then brightened to a relatively stable plateau (e.g., Kóspál et al. 2016). Our spectrum displays all the FUor characteristics discussed in Sect. 3.1.

V2494 Cygni: Also known as IRAS 20568+5217 and HH 381 IRS. The L1003 cloud in Cygnus is a region of active star formation (e.g., Magakian et al. 2010) with numerous HH objects, including HH 381 associated with IRAS 20568+5217 which illuminates a bright reflection nebula (Devine et al. 1997, Connelley et al. 2007). Reipurth & Aspin (1997) suggested the FUor nature of the object based on near-infrared spectra, a classification further supported by Greene et al. (2008) and Aspin et al. (2009b). The star brightened by $R \sim 2.5$ magnitudes sometime between 1952 and 1983 after which it seems to have reached a plateau (Magakian et al. 2013). The optical spectrum shows $H\alpha$ and forbidden emission lines originating from the HH 381 flow near the star, which has a projected length on the sky of 4.7 pc (Magakian et al. 2013, Khanzadyan et al. 2012). Our spectrum displays all the FUor characteristics discussed in Sect. 3.1.

V1057 Cygni: The star, which lies in a dense cloud within the North America Nebula (NGC 7000), brightened by 6 magnitudes in 1969 (Welin 1971a,b). A fortuitous pre-eruption low resolution optical spectrum taken in 1957 shows an "advanced T Tauri emission spectrum with no detectable absorption lines" (Herbig & Harlan 1971). The outbursting star was studied in detail photometrically and spectroscopically by Herbig (1977). The light curve from 1969 to 2012 has been compiled by Kopatskaya et al. (2013), who showed that the rapid decline in brightness can be fitted with an exponential curve. They also found that the I-band photometry has a strong 523-day periodic variation with ~ 0.5 mag ampli-

tude. V1057 Cyg has a high-velocity long-lasting wind which manifests itself through strong blueshifted absorption troughs at several prominent optical lines (Herbig 2009). Hartmann & Kenyon (1987) presented high resolution near-infrared spectra, which are consistent with the disk accretion model for FUors. Most recently, Green et al. (2016) have detected a faint companion to V1057 Cyg with a projected separation of 58 mas and a brightness difference of $\Delta K \sim 3.3$ mag. Our spectrum is discussed in Sect. 3.1.

V2495 Cygni: Also sometimes called the Braid Nebula Star. A bright near-infrared reflection nebula appeared between 1999 and 2001, brightening at K-band by at least 4 magnitudes (Movsessian et al. 2006). Their near-IR spectrum shows many characteristics of FUors (e.g. ‘triangular’ H-band continuum, strong water and CO absorption), and is essentially identical to the spectrum we show here. The source is associated with several HH objects, HH 629/635, with a projected length on the sky of 0.8 pc (Magakian et al. 2010, Khanzadyan et al. 2012). The object is highly extinguished, so our H-band spectrum is noisy and the J-band spectrum is missing. The CO absorption is very deep and the H-band continuum has a clear triangular shape.

V1735 Cygni: Also known as Elias 1-12, IRAS 21454+4718. and HBC 733. Elias (1978) showed that this object, located in the dark molecular filaments stretching $\sim 2^\circ$ west of IC 5146, had brightened by at least 5 visual magnitudes between 1952 and 1965, and identified it as a new FUor. Sandell & Weintraub (2001) found a bright submillimeter source, V1735 Cyg SM1, about 24 arcsec northeast of V1735 Cyg. SM1 is almost coincident with the IRAS source 21454+4718. Both sources were detected in X-rays with XMM-Newton by Skinner et al. (2009). Six out of seven of our spectra of this object are consistent with the spectrum shown in Greene & Lada (1996), demonstrating that the object is quite stable. However, one spectrum differs, and this spectroscopic variability is further discussed in Sect. 5.3. Our spectrum shows the FUor characteristics discussed in Sect. 3.1, with exceptionally strong water vapor features.

V733 Cephei: Also known as Persson’s Star. The outburst of this object was first noticed in 2004 (Persson 2004). Peneva et al. (2010) found that the earliest photographic plate showing the outburst was taken in 1971, and the object slowly rose in brightness until 1993. From 2007 to 2009, they observed this object to slowly fade. Optical and near-IR spectra (Reipurth et al. 2007) show great similarity to FU Ori, securing this object’s classification as a FUor. Our spectrum of V773 Cep is consistent with the spectrum shown in Reipurth et al. (2007).

4.2. FUor-like Objects

Wide-field and all-sky surveys are becoming increasingly common, and as a result it is more and more likely that a new FUor eruption will be quickly detected. Until recently, however, this was not the case, and hence we can be certain that in the past many FUor eruptions have been overlooked. Since some FUors retain their spectroscopic characteristics for up to a century or even more (e.g., FU Ori 1936 eruption, V883 Ori <1888 eruption), we expect to find a number of objects that have all the FUor characteristics, but whose outbursts were missed. A very similar situation exists for novae, for which the terms nova and nova-like object have been introduced, depending on whether an eruption has been witnessed or not. In analogy, Reipurth et al. (2002) suggested to use the nomenclature FUors and FUor-like objects. In this section, we list 10 objects which have clear spectroscopic FUor characteristics, but for which an eruption was missed. In Section 5 we compare the properties of bona fide FUors and the FUor-like objects. The de-reddened spectra of the FUor-like objects are presented in Figure 6.

RNO 1c: This heavily extinguished object is located ~ 6 arcsec from the FUor RNO 1b in the L1287 cloud. Unlike RNO 1b, however, no outburst has been observed. Based on a 2.291-2.298 μm spectrum, Kenyon et al. (1993) found that RNO 1c has the same deep CO absorption characteristic as FUors and, combined with its energy distribution, suggested its FUor nature. Our complete 1-4 μm spectrum mostly supports this conclusion. The spectrum shows strong, distinct CO band heads, although the ‘triangular’ H-band continuum resulting from water absorption that is a characteristic of FUors is quite weak.

PP 13S: Also known as IRAS 04073+3800. PP 13 is a small compact reflection nebula in the L1473 cloud in Perseus (Parsamian & Petrossian 1979). Cohen et al. (1983) found the nebula to be associated with two sources, PP 13N, a typical T Tauri star, and PP 13S, a cometary nebula with no $\text{H}\alpha$ emission and illuminated by an embedded infrared source. Further near-infrared imaging was presented by Smith (1993), who resolved PP 13N into a close binary. Sandell & Aspin (1998) and Aspin & Sandell (2001) found PP 13S to be driving a molecular outflow, and detected deep, broadened 2.3 μm CO absorption bands in a 2.0-2.5 μm spectrum, and on this basis suggested that PP 13S could be in an elevated FUor state. Aspin & Reipurth (2000) found a small Herbig-Haro jet, HH 463, emanating from PP 13S along the axis of the molecular outflow. Perez et al. (2010) presented CARMA $0''.15$ resolution 227 GHz observations of the circumstellar disk of PP 13S. Since 1998, the K-band magnitude has faded from 9.2 to 10.8. However, our data show that the spectrum in the K-band is little changed from 1998. There is still weak H_2 emission, presumably from HH 463, and the CO band heads are indistinct. At first glance the red featureless continuum is unlike any bona fide FUor, however, this is primarily due to the high extinction towards

the object. The water absorption bands that form the characteristic ‘triangular’ shape of the continuum become evident when the spectrum is dereddened by an A_V of about 56 mag.

L1551 IRS 5: This is a deeply embedded object (Fridlund et al. 1980), that was classified as a FUor on the basis of its optical spectrum seen via a reflection nebula (Mundt et al. 1985, Stocke et al. 1988). The source is a binary with projected separation of $0''.36$ (Bieging & Cohen 1985, Lim et al. 2016), with each component driving a jet (Fridlund & Liseau 1998, Rodríguez et al. 2003). The near-infrared spectrum in Reipurth & Aspin (1997) shows H_2 emission and CO band absorption. Strong [FeII] emission seen in our spectrum at $1.644 \mu\text{m}$ is unusual for FUors, but - as the H_2 emission - it likely derives from the associated jets. Greene et al. (2008) presented high-resolution near-infrared spectroscopy, and used cross-correlation with FU Ori to demonstrate their similarities: deep CO absorption, triangular H-band continuum, and strong break at $1.33 \mu\text{m}$.

Haro 5a IRS: This source, also known as IRAS 05329-0505, is one of the more luminous embedded sources in Orion (e.g., Wolstencroft et al. 1986). Haro 5a and Haro 6a designate the two lobes of an optically visible reflection nebula surrounding the IRAS source (Haro 1953). This is the source for the giant flow HH 41, 42, 128, 129, 294, and 295 (Reipurth et al. 1997a). The object was identified as a FUor-like object based on its near-IR spectrum (Reipurth & Aspin 1997). Our spectrum shows an extremely red continuum with strong CO absorption, and without photospheric absorption lines. The water absorption bands creating the triangular shape in the H-band appears to be weakly present, but when dereddened by an extinction of $A_V \sim 57$ mag, their presence become evident (see Figure 6).

IRAS 05450+0019: This is an embedded source also known as NGC 2071 MM3 which illuminates a large bipolar reflection nebula in the NGC 2071 region at a distance of 400 pc (Connelley et al. 2007). It was identified as a FUor-like object by Connelley & Greene (2010) based on its near-infrared spectrum, which shows very strong CO absorption and a triangular continuum shape in the H-band. Our present spectrum is identical to the earlier spectrum.

Z Canis Majoris: Herbig (1960) identified Z CMA as a young star, which he classified as a HAeBe star. Later, Hartmann et al. (1989) suggested that Z CMA is a FUor on the basis of weak CO absorption and doubled absorption lines from Li I and Ca I near 671 nm which they interpret as originating from a rotating accretion disk. The star also displays the wide blueshifted absorption troughs at the $H\alpha$ and Sodium doublet characteristic of FUors (e.g., Hessman et al. 1991, Welty et al. 1992). Both the HAeBe and the FUor classification turn out to be correct, since Z CMA has been found to be a $0''.1$ binary (e.g., Haas et al. 1993, Velazquez & Rodríguez 2001), where the SE component is a FUor and the NW component is a Herbig Be star (e.g., Bonnefoy et al. 2016). Z CMA drives a giant HH flow with a well

collimated jet (Poetzel et al. 1989). Whelan et al. (2010) demonstrated that this large-scale jet is driven by the Herbig Be star, but that also the FUor drives a small $\sim 0''.4$ jet, see also Antonucci et al. (2016). Z CMa shows major optical variability, Covino et al. (1984) collected the photometric history from 1923 to 1983, revealing an amplitude of 3 magnitudes, but no outburst, implying that it must have occurred prior to 1923. This variability has been traced to the Herbig Be component (e.g., Bonnefoy et al. 2016). Our near-infrared spectrum shows little resemblance to a FUor spectrum, which evidently is due to the superposition of the FUor spectrum with the (brighter) Herbig Be spectrum (both of which are separated in the integral field spectra of Bonnefoy et al. 2016). We note that the Br γ line is in emission with broad blue and red shifted wings extending out to $\pm \sim 1000 \text{ km s}^{-1}$, whereas the He I line only has a blue shifted absorption wing extending out to 1000 km s^{-1} .

BBW 76: Also known as V646 Puppis. This object was identified as a FUor based on its optical spectrum and near-IR photometry (Reipurth 1985b, Reipurth 1990). Photographic plates from 1900 show it as bright as it is today (Reipurth et al. 2002), rather than the usual slow decline observed from most FUors. Evans et al. (1994) did not detect a CO outflow at 346 GHz, and it is not associated with an HH object (Reipurth & Aspin 1997). Although the optical line profiles changed in observations obtained over a period of 10 years starting in 1985 (Reipurth et al. 2002), our spectrum of this target is consistent with the K-band spectrum 20 years earlier presented in Reipurth & Aspin (1997).

Parsamian 21: Also known as IRAS 19266+0932. The object, which displays a prominent reflection nebula (e.g., Connelley et al. 2007), was identified as a FUor by Staude & Neckel (1992) based on its optical spectrum and spectral energy distribution. The optical spectrum showed H α absorption blueshifted by $\sim 600 \text{ km s}^{-1}$, Li absorption, and an F5 giant spectral type. The near-IR spectra presented by Greene et al. (2008) and Connelley & Greene (2010), as well as our spectrum shown here, show a remarkable similarity to FU Ori and support the conclusion that this is a FUor-like object. The visible light brightness has not appreciably changed for at least 57 years (Semkov & Peneva 2010). SED analysis (Gramajo et al. 2014) and near-IR polarimetry (Kóspál et al. 2008) show that this target is seen nearly edge-on. We do not see a far-side (southern) reflection nebula for Parsamian 21, despite background stars being visible to the south. Parsamian 21 appears to be at the southern edge of its cloud, so it is likely that there is simply no dust to the south of Parsamian 21 to scatter light.

CB 230 IRS1: Also known as IRAS 21169+6804 or CB230 A. This is a deeply embedded Class 0/I protostar in the L1177 cloud. A companion, IRS2, is located $\sim 10''$ to the east (e.g., Massi et al. 2008), corresponding to about 3000 AU at the 300 pc distance (e.g., Das et al. 2015). High-resolution VLA observations reveal another close companion at $0''.3$

separation, making it a triple system (Tobin et al. 2013). No outburst has been witnessed. Massi et al. (2008) mention the possibility that some of the spectral features could be from a circumstellar disk, as in a FUor, but do not classify this object as a FUor. Our spectrum shows that the source shares prominent characteristics of FUors: strong CO absorption, ‘triangular’ H-band continuum, and a dearth of photospheric metal lines. Hence, we classify CB230 IRS1 as a new FUor-like object.

HH 354 IRS: Also known as IRAS 22051+5848 or L1165 SMM1. This is the source of a giant HH outflow (Reipurth et al. 1997a) and it illuminates a reflection nebula visible in the optical and near-IR (e.g., Connelley et al. 2007). HH 354 has a projected separation of 2.4 pc from IRAS 22051+5848 at the ~ 750 pc distance of the L1165 cloud (Reipurth et al. 1997a). The source is an embedded Class 0/I protostar, and Reipurth & Aspin (1997) showed that the K-band spectrum has a red featureless continuum and strong CO absorption, and noted that the K-band spectrum is very similar to L1551 IRS5. No outburst has been detected. The K-band brightness of this object has varied from $K=13.3$ in 1987 (Persi et al. 1988) to $K=9.7$ in 1999 (2MASS) to $K=10.8$ in this paper. Additional near-infrared spectroscopy supports the classification as a FUor-like object (Greene et al. 2008, Connelley & Greene 2010), and the spectrum we present here is consistent with previous spectra. High-resolution radio continuum VLA observations have revealed a $0'.3$ companion (Tobin et al. 2013).

4.3. Peculiar Objects with Some FUor Characteristics

A number of objects have been identified over the years as FUors, which either through closer comparison with the spectra of the three classical FUors (Section 3) or through spectral variability are no longer convincingly classifiable as FUors. In the following we comment on 8 such objects.

V1647 Orionis: The eruption of this object was discovered by the amateur astronomer Ian McNeil, when a bright reflection nebula, now known as McNeil’s Nebula, appeared in 2004 in the Lynds 1630 cloud (McNeil et al. 2004, Briceño et al. 2004). Near-IR spectra, taken shortly after the outburst was noticed, showed emission from the CO band heads near $2.3 \mu\text{m}$, atomic H, Na I, Ca I, and Ca II, and strong absorption from He I at $1.083 \mu\text{m}$, water ice, and solid state CO at $4.6 \mu\text{m}$ (Reipurth & Aspin 2004b, Vacca et al. 2004). After photometrically declining to pre-outburst brightness, V1647 Ori unexpectedly brightened again in August 2008 to be as bright as it was in 2004. During this second brightening, the near-IR spectrum was quite different than during its 2004 eruption. The spectrum showed strong water vapor absorption and ‘triangular’ H-band continuum common among FUors, $\text{Br}\gamma$ emission, and possible CO band head absorption (Aspin et al. 2009a). The Harvard

plate collection reveals that this object previously erupted in 1966-67 (Aspin et al. 2006). Our spectrum shows that atomic hydrogen and the CO bands are now back in emission, but other than that the overall spectrum is remarkably FUor-like. However, the presence of CO emission is such a major deviation from 'normal' spectroscopic FUor appearance that we do not include the object among the FUors. One possible, but unproved, explanation could be that V1647 Ori is a close binary with a FUor plus an active companion that causes the CO emission, a scenario reminiscent of Z CMa. Principe et al. (2017) mapped two distinct, misaligned molecular outflows, but do not find evidence for any companion at distances larger than 40 AU. If a companion is responsible for the recent outburst, however, it would still be close to periastron, and thus difficult to detect.

IRAS 06297+1021W: This IRAS source, located in the NGC 2264 clouds, is resolved at near-infrared wavelengths into two sources with a separation of $70''$ (Connelley et al. 2008a,b). A near-infrared spectrum of the western component was presented by Connelley & Greene (2010), who noted certain spectroscopic features characteristic of FUors, but also strong discrepancies. The continuum looks like a FUor, with a triangular H-band profile and He absorption. However, in common with V1647 Ori and Z CMa, it has CO in emission. Also similar to Z CMa, this object shows emission from sodium ($2.208 \mu\text{m}$), $\text{Br}\gamma$, $\text{Pa}\beta$, and the Ca IR triplet ($0.85 \mu\text{m}$).

AR 6a: Also known as V912 Mon. This is a bright near-infrared source in NGC 2264. While an outburst has not been observed in this object, Aspin & Reipurth (2003) suggested, based on a K-band spectrum showing strong CO and $\text{Br}\gamma$ absorption, a FUor-nature for AR 6a. However, our present spectrum, taken more than 10 years later, now shows only weak CO absorption and the Br series in absorption, giving the appearance of a highly reddened early type star. Notably there is no triangular shape of the continuum in the H-band. Since 2003, the spectrum of this object has evidently changed and it is no longer similar to a FUor.

AR 6b: This is a faint companion to AR 6a, at a separation of about $3''$. An outburst has not been observed. The K-band spectrum of Aspin & Reipurth (2003) shows stronger CO absorption and more IR excess than AR 6a. Aspin & Reipurth (2003) argue that this should be classified as a FUor due to the CO absorption and overall spectroscopic similarity to PP 13S. Our $1\text{-}2.5 \mu\text{m}$ spectrum shows high veiling, and possibly water absorption from 1.7 to $2 \mu\text{m}$, but the spectrum is too noisy to make definite statements on the presence of water. The individual CO bands are not distinct, possibly due to high rotation. The spectrum is certainly not one typical of T Tauri stars, and a FUor-like classification is still possible, but we feel it safer to withhold judgment until better data are in hand.

IRAS 06393+0913: Connelley & Greene (2010) obtained a SpeX near-infrared spec-

trum of this object in NGC 2264, and noted certain similarities to FUors, especially the very deep CO band head absorption, but due to the lack of any water absorption creating the triangular continuum shape in the H-band they stepped back from classifying the object as a FUor-like object. Moreover, as discussed in Section 7, the luminosity of this object is as low as $0.9 L_{\odot}$, which opens the question whether it might be a young brown dwarf, see Section 6.

V346 Normae: Also known as HH 57 IRS. The eruption was discovered in 1983 and the star is visible on plates taken as early as 1980 (Graham & Frogel 1985, Reipurth 1985a). Optical spectra taken at that time showed $H\alpha$ absorption blue-shifted by $\sim 440 \text{ km s}^{-1}$ and Li absorption. V346 Nor drives the little HH flow HH 57 (Prusti et al. 1993, Reipurth et al. 1997b). Ábrahám et al. (2004) compiled the light curve up to that time, and most recently Kraus et al. (2016) and Kóspál et al. (2017) noted that V346 Nor had declined significantly in brightness by 2010, indicating a drop in accretion rate by three orders of magnitude, followed by another brightening. Our spectrum is taken in July 2015 during this second brightening, but with the source still about 4 magnitudes fainter than during its previous outburst. It has been assumed up to now that V346 Nor is a bona fide FUor, mainly because of its brightening during the early 1980’s, but also due to its strong P Cyg profile at $H\alpha$ (e.g., Graham & Frogel 1985). However, our spectrum as well as one by Graham & Frogel (1985) show virtually no CO absorption, while another spectrum from the mid-1990’s (Reipurth et al. 1997b) shows pronounced CO emission and $\text{Br}\gamma$ emission (which also has disappeared again). Moreover, H_2 emission is now present in the spectrum. The unusual light curve and the spectroscopic variability makes V346 Nor more similar to V1647 Ori, and we similarly consider it to belong to the group of peculiar stars with some FUor characteristics. We speculate that also V346 Nor could be a binary with a FUor and an active companion, as the FUor-like object Z CMa.

IRAS 18270-0153W: This object was identified as a possible FUor-like object by Connelley & Greene (2010), showing a ‘triangular’ H-band continuum, strong CO absorption, and no photospheric absorption lines, with an appearance similar to other FUor-like objects. However, our more recent spectrum, although rather noisy, no longer looks like a FUor, showing weaker CO absorption and a smoother H-band continuum.

V371 Serpentis: Originally listed as EC 53 by Eiroa & Casali (1992), who noted a small cometary nebula in their infrared imaging survey of the Serpens core. Hodapp (1999) found the nebula to be variable, and Hodapp et al. (2012) determined a period of 543 days with an amplitude of $\Delta K \sim 2$ mag, possibly due to a very close companion, and also noted that the source has a resolved $0''.3$ companion. The high resolution spectra from Doppmann et al. (2005) of three segments in the K-band are consistent with our spectrum, which shows

CO absorption, triangular H-band continuum, and a dearth of identifiable photospheric absorption lines. Several emission lines of [FeII] and H₂ are seen which we ascribe to shocks in a small jet. The object is extremely red, so the H-band spectrum is noisy, and the J-band spectrum is absent despite 4 hours of integration. It is conceivable that V371 Ser could be a FUor-like object, but the data are not good enough to confirm that. Moreover, as we discuss in Section 7, there is the concern that V371 Ser has a luminosity of only 1.6 L_⊙, which should be divided between two or possibly three components. In Section 6 we discuss the possibility that V371 Ori is a newly born brown dwarf.

IRAS 18341-0113S: Similar to the previous object, this one was also identified as a possible FUor-like object by Connelley & Greene (2010), showing a ‘triangular’ H-band continuum, strong break in the continuum slope at 2.3 μm, but barely detectable CO absorption. Our new spectrum, however, no longer looks like a FUor, showing no appreciable CO absorption and a smoother red H-band continuum. We therefore include also this object in the category of peculiar objects with some FUor characteristics. We also note that IRAS 18341-0113S has a very low luminosity of only 0.8 L_⊙, in fact it is the lowest luminosity object of all our 33 targets, and in Section 6 we discuss the possibility that it may be a very young brown dwarf.

4.4. Spectral Variability of the Bona Fide FUors

FUors are much less spectroscopically variable than other YSOs, and their spectra maintain their FUor characteristics decades after the eruption. The only major spectroscopic change seen in a bona fide FUor is the strong weakening of the CO band in V1057 Cyg, which has accompanied its significant fading (Section 3.1). Connelley & Greene (2014) monitored two FUors (V1735 Cyg and V2494 Cyg, each observed 5 times) among 19 YSOs. The He I line at 1.08 μm (one of the few strong lines in a FUor spectrum) varied on average by 18% for the two monitored FUors, with a maximum variability of just under 60%. However, this line varied on average by 57% for the other YSOs, with a maximum variability of a factor of 12. In the course of this survey, 11 of the 33 targets were observed more than once in SXD mode. V1735 Cyg was the only target to show a significant change in this time.

Combining the data in Connelley & Greene (2014) with our new data, V1735 Cyg has been monitored with SpeX eight times over the past nine years. The spectrum showed little change (other than slight changes in the He I line profile) until July 8, 2016. The spectrum taken on that night was significantly redder (Figure 7), and the He I line showed a P Cygni profile for the first time (Figure 8). The additional flux appears to be a featureless red continuum, but with added CO absorption. The change in the CO and He I lines shows

that this was not a simple data processing error, or a change in the line-of-sight extinction. Before this event, the He I line showed blueshifted emission with a maximum velocity of -500 kms^{-1} to -800 kms^{-1} . This event accelerated the wind velocity up to -950 kms^{-1} . An observation taken the following month shows that V1735 Cyg had returned to its previous state. The He I and CO lines, as well as the continuum, were again consistent with previous spectra.

Despite the obvious spectroscopic changes during this unusual event, the K-band brightness of V1735 Cygni appears to have changed very little, if at all. The K-band flux on July 8, 2016 is consistent with our photometry from Aug 28, 2015, a year before this event. On the month after the event, the photometry on Aug 20, 2016 is only 0.2 magnitudes fainter than on July 8, 2016. Considering the very slight photometric change, it is unlikely that this event represents a new outburst or significant change in the state of this FUor. We seem to have caught a rare, isolated, and transient event that demonstrates that FUors *can* exhibit significant spectroscopic variability without much photometric variability.

5. FUors as Low-Gravity Objects

Figure 9 shows a comparison of the equivalent widths of the bluest CO band (measured from 2.292 to 2.320 μm) versus the sodium plus calcium lines of FUors, of some Class I sources, and of late field dwarfs, giants, and supergiants. It is readily seen that this diagram effectively differentiates FUors and FUor-like objects from the Class I sources. This diagnostic diagram has also been used by Greene & Lada (1996) and later by Connelley & Greene (2010). The Na (2.208 μm) and Ca (2.265 μm) lines were used, as they are near the CO band heads so they are all equally affected by veiling and extinction. In this figure, adding veiling tends to push a star closer to (0,0). Both bona fide FUors and FUor-like objects mostly lie in a tight group near the giant stars (and along the veiling vector from the supergiants) in Figure 9. This is consistent with the interpretation of FUors being low gravity objects. If we let m be the average equivalent width of the Na + Ca lines, then to be on the FUor side of the figure the CO equivalent width should be greater than $3m+5$ (shown by the gray dashed line). We note that the peculiar objects tend to mostly be located closer to (0,0) in a group separate from the majority of the bona fide FUors and FUor-like objects.

The separation into two distinct groups of FUors plus FUor-like objects vs. peculiar objects is broken by four of the 33 objects in Figure 10, and we discuss these four objects in the following:

- 1) The only bona fide FUor that clusters with the peculiar objects is V1057 Cyg. This

is unexpected and somewhat disturbing, since V1057 Cyg is one of the classical FUors which helped to define FUors as a class. As discussed in Section 3.1, V1057 Cyg has undergone a significant evolution in luminosity, with a concomitant major decrease in its CO band strength, which accounts for its location further left in Figure 10 than any other FUor or FUor-like object. We note that Calvet et al. (1991) show (their Fig.5) that CO absorption is only dominant in the outer annuli of the circumstellar disk. Hence as the disk cools and fades, the outer annuli may become undetectable. Or if the outer annuli are not continuously replenished from an envelope, they will spiral inwards. The explanation for its weaker sodium and calcium lines is even less clear, we speculate that hot spots due to accretion onto the stellar surface begins to dominate as the disk emission fades, thus increasing veiling. Whatever the specific reason, we believe that the location of V1057 Cyg outside the clump of FUors and FUor-like objects in Figure 10 is due to the recent rapid decay from its high FUor state.

2) The FUor-like object V371 Ser is also located among the peculiar objects and is close to V1057 Cyg in the diagram. The object is deeply embedded and is only seen as a reflection nebula, even at near-infrared wavelengths. This is in itself unlikely to be the cause of its location among the peculiar objects, since seven other objects are also so embedded that they are only seen as compact reflection nebulae. We have no explanation for the location of V371 Ser in the diagram.

3) Z CMa is located in the extreme lower left corner of Figure 10, but this is readily understood, since the object is a close binary combining a FUor and a Herbig Ae/Be star, where the latter dominates the light in the near-infrared.

4) IRAS 06393+0913 is located in the middle of the group of FUors and FUor-like objects in Figure 10. This is perhaps not surprising, since its main deviation from a FUor spectrum is the absence of broad water bands and those would not affect the line measurements used for the diagram.

Figure 3 shows that all of the bona fide FUors have a 'triangular' H-band continuum profile. As stated by Barman et al. (2011), the absorption bands of water naturally meet in the middle of the H-band, shaping the continuum into the well known triangular profile. As gravity increases, collisionally induced absorption (CIA) from H₂ increases, and CIA can be the dominant source of opacity at the higher gravity of dwarf stars (Borysow et al. 1997). CIA has a very broad wavelength dependence, effectively smoothing out the otherwise triangular profile into the more rounded profile seen in late type dwarfs. The ubiquity of a triangular H-band profile among bona fide FUors is further evidence in support of FUors being very low gravity objects.

6. Brown Dwarfs as FUor Impostors

Here we address the question of whether there are other objects in star forming regions that may mimic the spectra of FUors. Broadly speaking, FUors in the near-infrared have mid- to late-type M-spectra. The only other objects found in star forming regions with such spectra are young brown dwarfs. At an age of 1 Myr, the brown dwarf mass limit corresponds to a spectral type around M5.5. Figure 12 shows the near-infrared spectrum of FU Ori together with that of HBC 341 (Dahm & Hillenbrand 2017), a partly embedded M5 star bordering the brown dwarf regime with an age assumed to be roughly 1 Myr, and that of TWA-8B (Allers & Liu 2013), a brown dwarf in the 10-Myr old TWA association.

The similarity of the spectra is striking, and perhaps even surprising, given that the FUor spectrum is emitted by a disk, while the BD spectra presumably comes from a photosphere. The spectra are very similar even in most details, but there are a few differences. The first thing to notice is that the BD spectra show somewhat weaker CO bands, however, when a larger sample of young BDs and FUors are compared, the two distributions of CO strength do have some overlap, which makes it unusable as a criterion for distinction.

Paschen- α is very pronounced in FU Ori, and much weaker in HBC 341, but its location in a region of limited atmospheric transmission makes it a poor criterion. Paschen- β , however, is better placed, and shows much higher strength compared to BDs. Figure 13 shows a histogram of equivalent widths of Paschen- β for the FUors and FUor-like objects vs a number of young BDs in the TW Hya association. In this figure, the number of objects at a given EW is the sum of the objects whose EW range of uncertainty included that EW value. These EW distributions just overlap due to a single FUor-like object, BBW 76. Z CMa shows strong emission at the Paschen- β line, and is off to the far left in the figure.

A set of weaker lines in the J-band also show certain differences. The Na doublet at 1.138/1.141 is pronounced in BDs, but is absent in FU Ori. Other doublets of potassium (1.169/1.178 and 1.243/1.253) and aluminum (1.313/1.315) are stronger in BDs than in FU Ori, as are some iron lines (1.169/1.177/1.189/1.198). However, the fact that many FUors are highly extincted makes the J-band often difficult to observe.

In summary, for a purely spectroscopic classification, the Paschen- β strength is the best, although not completely unique, way to distinguish between a FUor and a BD.

In this context, two interesting questions arise: can brown dwarfs undergo FUor eruptions? And if so, how can we distinguish between a substellar object with and without major accretion?

Regarding the first question, we note that brown dwarfs are formed like stars, except

that they fail to reach the hydrogen-burning limit because either their mass reservoirs are not large enough (Padoan & Nordlund 2004) or they are prematurely expelled from their cloud core by companions (Reipurth & Clarke 2001) or their mass reservoir is destroyed by a nearby massive star (Whitworth & Zinnecker 2004). All three mechanisms are likely to operate, although identifying which mechanism is responsible for a given object is most likely not possible. The key is that in all three cases there is a smooth transition of properties across the stellar/substellar limit. We know that stars with a mass as low as an early M-type star can erupt as a FUor (Reipurth, in prep.), so there seems little reason why a slightly less massive brown dwarf also cannot undergo a FUor outburst. Additionally, we know that brown dwarfs have circumstellar disks, albeit smaller than those of higher-mass T Tauri stars (e.g. Testi et al. 2016). We conclude that there is no obvious reason why brown dwarfs should not undergo FUor eruptions like their higher-mass brethren, although they may perhaps not reach as high luminosities.

Regarding the second question, as we have shown above, the photospheric spectra of brown dwarfs and the disk spectra of FUors are almost indistinguishable at the resolution employed here. Future higher resolution spectroscopy may be key to separate the two types of objects, e.g. by looking for the double-lined profiles characteristic of rotating disks in FUors (e.g., Hartmann & Kenyon 1996). Meanwhile it appears that luminosity is a necessary parameter to separate brown dwarfs from brown dwarfs undergoing FUor outbursts. However, setting a limit in luminosity between brown dwarfs and brown dwarfs in a FUor state may not be straightforward, since young brown dwarfs are likely to experience a continuum in accretion luminosity.

In Section 7 we determine the luminosities of all 33 objects of this study. The three lowest-luminosity objects are IRAS 06393+0913 ($0.9 L_{\odot}$), V371 Ser ($1.6 L_{\odot}$), and IRAS 18341-0113S ($0.8 L_{\odot}$). We have classified all three as peculiar, and they are individually described in Section 4.3. With such low luminosities, and their spectra having some features reminiscent of FUors, these spectra may be from a photosphere of a very low mass object with at most a modest contribution from accretion.

7. Bolometric Luminosity Distribution

We now discuss the bolometric luminosities of FUors, and to that end their distances are important. The distances we use are listed in Table 2 together with references to the distance determinations. Although a few FUors have well determined distances, generally they are not well known, and in some cases are little more than wishful thinking. We have critically reviewed each distance, taking into account the many new accurate distance determinations

of star forming regions in recent years. See Appendix B for a discussion on the adopted distance to each star forming region.

We have estimated the bolometric luminosity for each target using the distances listed in Table 2. In an attempt to make a homogeneous set of luminosity estimates, we used publicly available photometry from 2MASS (JHK), WISE (3.4 to 22 μm), and Akari (65 to 160 μm). For the longer wavelengths of the spectral energy distributions (SED), we appended a 20 K blackbody for each object, scaling the blackbody curve to match the Akari 160 μm photometry. The 20 K temperature was chosen as that temperature provides a smooth transition from the measured SED to the extrapolated blackbody. The 20 K blackbody ‘tail’ on average adds 9% to the bolometric luminosity of the objects. We have not attempted to correct the photometry for extinction.

The bolometric luminosity distribution is shown in Figure 14. FUors are shown in red, FUor-like objects in blue. The median bolometric luminosity for bona fide FUors is $99 L_{\odot}$ and for FUor-like objects it is $35 L_{\odot}$. If taken at face value, the smaller value for the FUor-like objects could be understood under the assumption that FUors decline in brightness, and that the eruptions of some FUor-like objects may have taken place long ago, before the sky was well patrolled. However, a 2-sample K-S test shows that the bolometric luminosity distributions cannot be differentiated at the 90% confidence level, and we thus cannot show that these two distributions are statistically different.

We note that, despite being a spectroscopically rather homogenous group, FUors and FUor-like objects span a wide range of bolometric luminosities. Their luminosities span 3 orders of magnitude, from $\approx 6 L_{\odot}$ to $\approx 3500 L_{\odot}$. It has been widely assumed that FUors have considerable luminosities, but evidently some objects have luminosities that are only slightly brighter than typically found for classical T Tauri stars, despite their dramatically different spectra.

8. Conclusions

We have conducted a homogeneous near-IR spectroscopic survey of all currently known FUor and FUor-like YSOs as well as some peculiar objects with certain FUor characteristics, in total 33 objects with varying degrees of evidence that they are indeed FUors. Our goal was to decide the nature of these objects by more stringent means. We have obtained the following results:

1. First we have determined the near-infrared spectroscopic characteristics of the three classical FUors FU Ori, V1057 Cyg, and V1515 Cyg in order to establish a set of reference

criteria. The main near-infrared spectral characteristics of these objects is deep CO band absorption, weak metal absorption lines, pronounced water vapor at the short and long sides of the H-band window giving rise to a characteristic triangular H-band continuum, a strong break at $1.32 \mu\text{m}$ due to water vapor, strong He I absorption (frequently blueshifted) at $1.083 \mu\text{m}$, and few if any emission lines.

2. We then applied these criteria to the 33 objects, and divided them into three categories: bona fide FUors (objects that display the above characteristics and for which an eruption was observed), FUor-like objects (which display the above characteristics but for which an eruption was not witnessed), and peculiar objects which either miss some FUor characteristics or display additional unusual features.

3. We examined multiple spectra of three FUors (V1057 Cyg, V1735 Cyg, and V2494 Cyg). V1057 Cyg has in recent years seen a significant weakening of the CO bands, possibly related to a steep fading in brightness. Of the eight spectra of V1735 Cyg obtained over the past 9 years, only one deviates from an otherwise stable appearance, one night showing an additional red continuum and stronger CO band absorption, with no significant change in brightness. V2494 Cyg showed no spectral variability.

4. We have plotted the equivalent widths of the $\sim 2.2 \mu\text{m}$ lines of Na and Ca versus the equivalent width of CO for all observed objects. FUors and FUor-like objects do not fall in the same area as Class I sources, but are found together with giant and supergiant stars, supporting other evidence that FUors are low-gravity objects. With only a few exceptions, the FUors and FUor-like objects are located together in a group, whereas the peculiar objects are mostly displaced to another nearby region of the diagram.

5. Whereas the first FUors to be discovered were bright optically visible stars, in recent years an increasing number of FUors are found that are embedded. Extinction is therefore an important parameter in the study of FUors, and we have estimated the amount of extinction for all FUors and FUor-like objects. We assume that any spectral differences between FUors are dominated by extinction rather than spectral differences and/or veiling. We then matched the slope of all FUors and FUor-like objects to FU Orionis, which has a low extinction of $A_V \sim 1.5 \pm 0.2$. Many of the objects were also observed in the L-band, and often show a pronounced $3 \mu\text{m}$ ice band. By measuring the depth of the ice band and comparing to the estimated extinction we have calibrated the relationship between the ice band optical depth τ and the visual extinction: $\tau = 0.048 * A_V - 0.13$.

6. Most FUors display reflection nebulae, and we provide an atlas of K-band images of the surroundings of all of the objects studied. We note that three objects have no optical counterpart and yet do not have pronounced reflection nebulae at K-band. We speculate

that these objects may not be deeply embedded, but merely located on or just beyond the back side of their clouds.

7. The near-infrared spectra of FUors and the more massive brown dwarfs display great similarity, and at low resolution can be indistinguishable. Close examination of their spectra show some discrepancies. Paschen- α is very pronounced in FU Ori, but is located in a region with poor atmospheric transmission. Paschen- β on the other hand is much stronger in FUors than in brown dwarfs, where it is often absent. Certain weak metallic lines in brown dwarfs are much stronger than in FUors, but both Paschen- β and these lines are in the J-band, which makes them hard to detect in highly extinguished objects. It is likely that also brown dwarfs can undergo FUor eruptions, and this may add to the confusion between brown dwarfs and FUors.

8. We have estimated the bolometric luminosity for each target using a homogeneous data set consisting of photometry from 2MASS (JHK), WISE (3.4 to 22 μm), and Akari (65 to 160 μm), and from the 160 μm data point we appended a 20 K blackbody. In view of the major improvement in distances to star forming regions in recent years, we review for each object its most accurate distance. The median bolometric luminosity for bona fide FUors is 99 L_{\odot} and 35 L_{\odot} for the FUor-like objects. Given that FUors decline with time and that FUor eruptions are more likely to be witnessed today than at earlier times, the difference is not unexpected. However, a 2-sample K-S test shows that the distributions cannot be distinguished at the 90% level.

9. We have confirmed two new FUor-like objects, V371 Ser and CB230 IRS1, that initially attracted attention due to their bright near-infrared cometary reflection nebulae. We classify V1647 Ori, frequently considered a FUor, as a peculiar object with some FUor characteristics since its spectrum differs significantly from that of FUors. We speculate that the object is a close binary with one component being a FUor and the other being responsible for the emission line spectrum. Similarly, V346 Nor has long been classified as a FUor, but its unusual light curve, its almost complete lack of CO absorption and presence of emission lines points to a peculiar nature, possibly another case of a close binary. Finally both AR6a/6b are deemed peculiar, in the case of AR6a because its spectrum has changed and is no longer FUor-like.

We are grateful to Nuria Calvet for a critical reading of an early version of the manuscript, to Will Best for providing spectra of brown dwarfs, to Scott Dahm for the spectrum of HBC 341, to Maria Kun for information on the distance of the L1287 cloud, to Adwin Boogert for information on water ice absorption, and to the anonymous referee for a help-

ful report. We acknowledge the support of the NASA Infrared Telescope Facility, which is operated by the University of Hawaii under contract NNH14CK55B with the National Aeronautics and Space Administration, and we are grateful for the professional assistance from Dave Griep, Eric Volquardsen, Brian Cabreira, Tony Matulonis, and Greg Osterman. This research has made use of the SIMBAD database, operated at CDS, Strasbourg, France, and NASA’s Astrophysics Data System. This publication makes use of data products from the Two Micron All Sky Survey, which is a joint project of the University of Massachusetts and the Infrared Processing and Analysis Center/California Institute of Technology, funded by the National Aeronautics and Space Administration and the National Science Foundation. This research has made use of NASA’s Astrophysics Data System.

Facilities: IRTF.

A. Extinction and Reflection Nebulae

FUors are generally associated with interstellar material, and especially among the more recently discovered ones there are a number of embedded cases. It is of interest to estimate the amount of extinction that each FUor suffers along our line of sight, and we use our spectral library to make such an attempt. As can be seen from Figure 3, FUor spectra have fundamental similarities. On the assumption that their difference in spectral slope is dominated by extinction rather than intrinsic spectral differences, we have determined the amount of extinction that must be added to the spectrum of FU Ori to make the best fit to the observed spectra of the other 32 objects studied here. We adapted the spectral fitting code used by Connelley & Greene (2010), using FU Ori as the reference star, and only considering extinction and not adding any veiling. This code adds extinction to the spectrum of FU Ori in an effort to minimize the RMS error between that model and the spectrum of the FUor in question. The estimated uncertainty in the extinction is the amount of change in extinction required to double the RMS fitting error between the FUor in question and the extinguished spectrum of FU Ori.

Herbig (1977) concluded that FU Orionis has very little extinction, and Hartmann & Kenyon (1985) and Kenyon et al. (1988) suggested an A_V of 1.55 and 2.2, respectively, by comparison with disk models. More recently, Zhu et al. (2007) determined an A_V of 1.5 ± 0.2 from a detailed comparison of observations with models, a value which we adopt here. Table 2 lists the derived extinctions for each object after adding FU Ori’s 1.5 magnitudes of extinction, and Figures 3 and 6 show the dereddened spectra. Two comments are pertinent: (1) Most of the objects in this study have a rather strong spectral similarity to FU Ori, thus giving some confidence in the estimated extinction values, but evidently the more discrepancies to FU Ori that a spectrum shows, the more uncertain the value becomes; (2) the extinction estimates refer to the light that reaches us, which may not always be dominantly from the source itself, but could be from reflected light that escapes through a cavity in those cases where the source is deeply embedded. Thus, the listed extinctions may be lower limits.

In order to evaluate whether we see a FUor directly, or we observe a compact reflection nebula, we have examined the K-band images that were obtained at the same time as each spectrum; Table 2 lists the corresponding K-magnitudes. Figure 11 shows panels with these K-band images. It is immediately clear that not all objects have stellar point spread functions. The following eight sources are not seen directly even in the K-band, but are compact reflection nebulae: L1551 IRS5, Haro 5a IRS, IRAS 05450+0019, V371 Ser, Parsamian 21, V2495 Cyg, CB 230 IRS1, and HH 354 IRS. All of these, with the puzzling exception of Parsamian 21, are among the objects with highest extinctions, which demonstrates that the

path of light from each source passes copious amount of dust.

It is well known that FUors in optical light are surrounded by often prominent reflection nebulae (e.g., Herbig 1977, Goodrich 1987). Indeed, CB230 IRS1 and V371 Ser were initially suspected of being FUor-like on account of their nebula morphology alone; their true nature was confirmed by subsequent spectroscopy. The reflection nebulae on larger scales are obviously more pronounced at short wavelengths, but these near-infrared images offer insight into the immediate surroundings of the objects. We note that ten objects do not show evidence for reflection nebulae in the K-band, these are: V883 Ori, V2775 Ori, FU Ori, IRAS 06297+1021W, IRAS 06393+0913, Z CMa, BBW 76, V1515 Cyg, V1735 Cyg, and V733 Cep. All of these objects are among the ones with lowest extinctions, although in three cases it is not negligible. The remainder show various degrees of reflection nebulosity. In eight cases we clearly see cometary nebulae with the source embedded at the apex, indicating that it is illuminating an outflow cavity. Perhaps not surprisingly, those eight are the same sources listed above that are not seen directly.

Only three sources do not show any sign in the visible of either a star or a reflection nebula. This is evidence of how the detection of FUors until recently has been primarily done in the optical. Since all of the sources are associated with dark clouds, it follows that almost all of these objects are located on the side of the clouds facing towards the observer. We note that *all* optically visible FUors and FUor-like objects are associated with an optical reflection nebula. A roughly equal number of objects should be located on the far side of dark clouds. Three sources without any optical counterpart, V2775 Ori, IRAS 06297+1021W, and IRAS 06393+0913, do *not* show evidence of reflection nebulae, suggesting that they are not deeply embedded, and these three objects may thus be part of the missing population of FUors that are located near the backside of clouds (we note that a weak reflection nebula around V2775 Ori was detected in an HST image, see Fig. 2 of Fischer et al. 2012).

Our extinction estimates along with our 2 to 4 μm spectra allow us to calibrate the relationship between the 3.0 μm ice band depth and the visual extinction for our sample of YSOs. The relationship between the depth of the 3.0 μm ice band and extinction is well established. Beck et al. (2001) showed that the 3.0 μm absorption is much greater towards T Tau S than T Tau N, consistent with T Tau S being seen through greater extinction. Beck (2007) fit an ice absorption model to 2 to 4 μm spectra of several YSOs. However, she considered the applicability of the relation between ice column density and visual extinction to be questionable. Chiar et al. (2011) clearly showed a linear trend between 3.0 μm ice band depth and the visual extinction through a quiescent dark cloud.

We adopted an empirical approach towards calibrating the relationship between the 3.0 μm ice band depth and the visual extinction. We measured the continuum flux at

2.50, 3.05, and 3.80 μm over a bandwidth of 0.05 μm . We fit a line between the 2.50 and 3.80 μm flux levels, and calculated the interpolated 3.05 μm continuum level (Figure 15). The relationship between A_v (derived by comparison to FU Ori) and the ice band depth is shown in Figure 16. For this figure, we used all of the FUors and FUor-like objects for which we have 2 to 4 μm spectra except for Z CMa, since its continuum is so unlike other FUor-like objects. The data in red are objects affected by reflection nebulae in the near-IR. Most of the very highly extinguished objects have reflection nebulae, and are affected by scattered light. The depth of the ice band appears to saturate near $\tau \approx 2$, corresponding to a visual extinction of about 30. Despite having sources seen through higher extinction, the ice band depth does not appreciably deepen for these highly extinguished objects. We fit a linear regression line through the data of all but the two highest extinction objects, for which the ice band optical depth appears to have saturated. We derive the following the relationship:

$$\tau = (0.048 \pm 0.008) * A_V - (0.13 \pm 0.14) \tag{A1}$$

where τ is the ice band optical depth and A_V is the visual extinction in magnitudes. τ was calculated as $-\ln(\text{flux at } 3 \mu\text{m}/\text{continuum at } 3 \mu\text{m})$

This method of calculating the ice band optical depth does not go to zero at zero extinction, due to a natural curvature in the spectrum of a FUor at this wavelength range. This curvature of the continuum is also seen among late M-giants in the SpeX library. To compensate for this effect, we subtracted the τ of FU Ori (likely the lowest extinction target) from all of the sources, and this is reflected in the equation above. Some objects strongly deviate from this relationship, such as Parsamian 21, which is a low extinction object (the reflection nebula is seen in visible light) but has a strong ice band absorption feature. In this case, a large fraction of the light from Parsamian 21 may be scattered, and the true extinction to the source may be much higher.

B. Comments on Adopted Distances

L1287. The two sources RNO 1b/c are found in Cassiopeia and are associated with the L1287 cloud located in the Orion arm of our Galaxy (Kun 2008). These sources are commonly assumed to be at the kinematic distance of 800 pc (Persi et al. 1988). However, recently Reid et al. (2014) used the VLBI to measure the parallax of a maser source in the L1287 cloud, and determined a distance of 930 ± 35 pc, which we henceforth use.

The California Molecular Cloud. The FUor-like object PP13S is located in a dense

core named L1473 within the giant California Molecular Cloud. A variety of distances have been determined for different components of the California Molecular Cloud, the most recent is the extinction-based study by Lada et al. (2009) suggesting a distance of 450 ± 23 pc, which we adopt here.

L1551. The small cloud L1551 in Taurus is located just south of the large Taurus cloud complex. Only three degrees from L1551 and also south of the Taurus complex is a similar small cloud containing the eponymous T Tauri. For T Tauri a VLBA distance of 146.7 ± 0.6 pc has been determined by Loinard et al. 2007, and we here assume the same distance for L1551, but adopt a greater uncertainty, 147 ± 5 pc.

Orion. The structure of the large Orion complex of star forming regions is increasingly well understood, see Bally (2008) for a review. Recently Kounkel et al. (2017) observed 36 YSOs with the Very Large Baseline Array (VLBA) and determined a distance to the Orion Nebula Cluster of 388 ± 5 pc (in excellent correspondence with the earlier, less accurate measurements of Jeffries 2007, Sandstrom et al. 2007 and Mayne & Naylor 2008) and found that the L1641 (Orion A) cloud is inclined away from us, with a distance of 428 ± 10 pc towards its southern portion, while similarly the L1630 (Orion B) cloud is increasingly distant towards the north, with NGC 2068 at 388 ± 10 pc and NGC 2024 at roughly ~ 420 pc. Consequently we adopt 428 pc for V2775 Ori, which is located in the southern part of L1641, and 388 pc for V883 Ori which is located in the northern part of L1641 near the ONC. For Haro 5a IRS in OMC 2 we also adopt the ONC distance of 388 pc, and the same for V1647 Ori just south of NGC 2068 and for IRAS 05450+0019 in NGC 2071 just north of NGC 2068. Due to plasma radio scattering in the λ Ori region, Kounkel et al. were not able to measure sources in that region, hence for FU Ori the best distance estimate remains the 400 ± 40 pc of Murdin & Penston (1977). FU Ori was measured by Gaia, but the First-Release value of 353^{+82}_{-56} pc is still not a significant improvement, so for now we remain with the 400 pc value.

NGC 2264. Four of the objects in this study are located towards NGC 2264, these are IRAS 06297+1021W, IRAS 06393+0913, and AR6a/b. Hence we re-examine the current status of distance estimates to this region. NGC 2264 is often assumed to be at a distance of about 800 pc, although various determinations range from 700 pc to 950 pc, see Table 1 in Dahm (2008) for a full summary. Subsequent distance determinations of the cluster are by Baxter et al. (2009), who suggest 913 ± 40 pc based on model fits to the rotational velocity distribution, Turner (2012) who suggests 777 ± 12 pc based on main sequence fitting to 13 B-type stars, and Kamezaki et al. (2014), who find 738^{+57}_{-50} pc based on VLBI parallax measurements of two water maser sources. Reviewing these values and their uncertainties, we deem that the 738 pc distance for now remains the best value for NGC 2264.

Monoceros. The two FUors V900 Mon and V960 Mon are found in this region. For V900 Mon we adopt the distance of about 1100 pc suggested by Reipurth et al. (2012). For V960 Mon there is much uncertainty about the distance, Caratti o Garatti et al. (2015) and Kóspál et al. (2015) assume 450 pc. However, this FUor is associated with the L1649/1650 cloud complex, for which Kim et al. (2004) derive a kinematic distance of 1100 pc, and we adopt that distance here.

Serpens. The three objects V371 Ser, IRAS 18270-0153W, and IRAS 18341-0113S are all located within the Serpens constellation, but in three different regions. V371 Ser is embedded in the densest part of the Serpens Core, which has frequently been assumed to be rather nearby, e.g. Straizys et al. (1996) determined that extinction rises at a distance of about 259 ± 37 pc. However, a more recent VLBA parallax study by Dzib et al. (2010) of a young binary in the Serpens Core indicated a distance of 415 ± 5 pc, later refined to 429 ± 2 pc (Dzib et al. 2011). This was supported by additional VLBA observations that yielded a distance of 436 ± 9 pc (Ortiz-León et al. 2016). This suggests that the Serpens Core is not part of the nearby Aquila Rift, but is located behind it, and the earlier extinction-based estimates most likely refer to the Aquila cloud complex. IRAS 18270-0153W is located in the northernmost cloud core in the filamentary cloud that contains the embedded Serpens-South cluster (see Figure 1 of Friesen et al. 2016). It has long been assumed that Serpens-South and the neighboring W40 star forming region are physically associated due to their similar gas radial velocities. Several stars in W40 were included in the parallax study of Ortiz-León et al. (2016), and it thus follows that Serpens-South is likely to be at a distance of 436 ± 9 pc, which we therefore also adopt as the distance to IRAS 18270-0153W. For the third object in Serpens, IRAS 18341-0113S, there is, however, no evidence that it is associated with the more distant clouds, and at its location on the southeastern edge of the Aquila Rift (see Figure 1 of Ortiz-León et al. 2016), it seems more likely that it is part of the Aquila Rift at the 259 ± 37 pc distance of Straizys et al. (1996), which we thus adopt

Aquila. The FUor Parsamian 21 has a very poorly determined distance, with suggestions varying from 400 pc (e.g., Kóspál et al. 2008) to 1800 pc (Staude & Neckel 1992). The object is located towards Cloud A of Dame & Thaddeus (1985), who suggest a kinematic distance of 500 pc. For lack of better determinations, we here adopt a distance of 500 pc, while recognizing its considerable uncertainty.

North America Nebula. The two FUors V1057 Cyg and HBC 722 are located towards the North America Nebula (NGC 7000), which together with the Pelican Nebula (IC 5070) form a single large HII region W80 that is bifurcated by the L935 dark cloud. Numerous distance determinations have been made over time, and we here adopt 550 ± 50 pc as determined by Laugalys et al. (2006). This distance is likely to apply to V1057 Cyg,

which is seen towards the northern part of the HII region. For HBC 722, which is located on the frontside of the L935 cloud, it is possible that the distance is slightly closer, but we also retain 550 pc for this object.

Khavtassi 141. The two FUors V2494 Cyg and HH 381 IRS are located in the L1003 cloud in Cygnus. Together with the nearby L988 cloud they form the two highest extinction regions in the large cloud Khavtassi 141, sometimes called the Northern Coalsack. Kh 141 is located within the Cyg OB7 association, with which it is assumed to be associated. Numerous distance estimates towards this region have been made, resulting in values from 500 to 800 pc; for details see the discussions in Herbig & Dahm (2006) and Khanzadyan et al. (2012). Following Herbig & Dahm (2006) we accept 600 pc as a compromise value.

IC 5146. V1735 Cyg is located towards the western part (L1045) of a long filamentary cloud which at its eastern extremity harbors the star forming region IC 5146. Starting with the study of Walker (1959) almost all studies have suggested a distance between 900 and 1200 pc (see Table 1 of Harvey et al. 2008) except Lada et al. (1999) who used extinction measurements to suggest a distance of 460 ± 60 pc. Upon reviewing the various methods, we adopt the distance proposed by Harvey et al. (2008) of 950 ± 80 pc.

L1165. The FUor HH354 IRS is embedded in the small cloud L1165, which is located east of the HII region IC 1396, at a separation of 2.6° . It is unclear whether or not the two are physically associated. The distance to IC 1396 has been determined as 870 ± 80 pc by Contreras et al. (2002), consistent with previous estimates (e.g. $\sim 1000 \pm 100$ pc by Garrison & Kormendy 1976). However, the CO local standard of rest velocity is discrepant, and hence it has been suggested that L1165 may form a foreground cloud, with a distance variously assumed between 200 pc and 400 pc (for a discussion, see Kun et al. 2008). HH354 IRS is associated with a maser, so an accurate distance may one day be measured, but until then we adopt a distance of 300 pc (e.g. Dobashi et al. 1994).

C. Objects sometimes considered FUors, but not included here

We here mention three objects which occasionally appear in lists of FUors but which we exclude in this study for the reasons stated.

Re 50 IRS1: Strom & Strom (1993) suggested that this embedded source is a FUor based on the $H\alpha$ profile seen via reflected light. Re 50 is a complex reflection nebula that appeared in the southern part of the L1641 cloud sometime between 1955 and 1979. It is illuminated by the embedded IRAS source 05380–0728, with a luminosity of $\sim 250 L_\odot$, and a spectrum of the associated reflection nebula shows $H\alpha$ and the Ca triplet in emission

(Reipurth & Bally 1986). Recently the northern part of the reflection nebula, Re 50N, closest to the source has brightened considerably, suggesting the possibility of a FUor eruption, but a near-infrared spectrum shows only a steeply rising featureless continuum (Chiang et al. 2015). While it is possible to imagine scenarios in which heated dust could swamp a FUor spectrum, we consider the absence of near-infrared spectroscopic features characteristic of FUors as disqualifying for a FUor classification.

OO Ser: This is a deeply embedded young star that erupted before 1994, but which faded almost back to its pre-outburst brightness in only 5 - 7 years (Hodapp et al. 2012), a timescale that places this object between the FUors and the EXors. A K-band spectrum obtained in 2006 showed no CO absorption bands (Kóspál et al. 2007).

V1331 Cyg: This luminous emission-line T Tauri star has occasionally been found in lists of FUors. It was Welin (1976) who first suggested that V1331 Cyg might be in a *pre-FUor* state, based on the similarity of its spectrum to the pre-outburst low-dispersion objective prism spectrum of V1057 Cyg obtained by Herbig (1977). While V1331 Cyg indeed has very strong winds and P Cygni profiles with deep absorption troughs on certain optical lines (e.g., Petrov et al. 2014), its rich emission line spectrum, including the 2- μ m CO bands in emission (Carr 1989), is completely different from all known FUors, and any speculations on a relation to FUors remain just speculations.

REFERENCES

- Ábrahám, P., Kóspál, Á., Csizmadia, S. et al., 2004, *A&A*, 428, 89
- Allers, K., & Liu, M., 2013, *ApJ*, 772, 79
- Antoniucci, S., Podio, L., Nisini, B. et al., 2016, *A&A*, 593, L13
- Ambartsumian, V.A., 1971, *Astrophysics*, 7, 331
- Armitage, P., Livio, M., Pringle, J., 2001, *MNRAS*, 324, 705
- Armond, T., Reipurth, B, Bally, J., & Aspin, C., 2011, *A&A*, 528, 125
- Aspin, C. & Reipurth, B., 2000, *MNRAS*, 311, 522
- Aspin, C. & Reipurth, B., 2003, *AJ*, 126, 2936
- Aspin, C. & Sandell, G., 2001, *MNRAS*, 328, 751
- Aspin, C., Reipurth, B., Beck, T., et al., 2009a, *ApJ*, 692, L67
- Aspin, C., Beck, T.L., Pyo, T.-S. et al., 2009b, *AJ*, 137, 431
- Aspin, C., Barbieri, C., Boschi, F., et al., 2006, *AJ*, 132, 1298
- Audard, M., Abraham, P., Dunham, M.M. et al., 2014, in *Protostars and Planets VI*, eds. H. Beuther et al., Univ. Arizona Press, p.387
- Bally, J. 2008, in *Handbook of Star Forming Regions Vol. I*, ed. Bo Reipurth, ASP, p. 459
- Baraffe, I., Vorobyov, E., Chabrier, G. 2012, *ApJ*, 756, A118
- Barman, T., Macintosh, B., Konopacky, Q., & Marois, C., 2011, *ApJ*, 733, 65
- Baxter, E.J., Covey, K.R., Muench, A.A. et al., 2009, *AJ*, 138, 963
- Beck, T.L. & Aspin, C. 2012, *AJ*, 143, A55
- Beck, T., 2007, *AJ*, 133, 1673
- Beck, T., Prato, L., & Simon, M., 2001, *ApJ*, 551, 1031
- Bell, K.R. & Lin, D. 1994, *ApJ*, 427, 987
- Bieging, J.H. & Cohen, M. 1985, *ApJ*, 289, L5

- Bonnefoy, M., Chauvin, G., Dougados, C. et al., 2017, *A&A*, 597, A91
- Bonnell, I. & Bastien, P. 1992, *ApJ*, 401, L31
- Borysow, A., Jørgensen, U., & Zheng, C., 1997, *A&A*, 324, 185
- Briceño, C., Vivas, A.K., Hernández, J. et al., 2004, *ApJ*, 606, L123
- Calvet, N., Patiño, A., Magris, G., & D’Alessio, P., 1991, *ApJ*, 380, 617
- Caratti o Garatti, A., Garcia-Lopez, R., Scholz, A. et al., 2011, *A&A*, 526, L1
- Caratti o Garatti, A., Garcia Lopez, R., Ray, T.P. et al., 2015, *ApJ*, 806, L4
- Carr, J.S. 1989, *ApJ*, 345, 522
- Chiang, H.-F., Reipurth, B., Walawender, J. et al., 2015, *ApJ*, 805, L54
- Chiar, J., Pendleton, Y., Allamandola, L., et al., 2011, *ApJ*, 731, 9
- Cieza, L.A., Casassus, S., Tobin, J. et al., 2016, *Nature*, 535, 258
- Clark, C., Lodato, G., Melnikov, S., & Ibrahimov, M., 2005, *MNRAS*, 361, 942
- Cohen, M., & Kuhl, L., 1979, *ApJS*, 41, 743
- Cohen M., Aitken D. K., Roche P. F., Williams P. M., 1983, *ApJ*, 273, 624
- Connelley, M., Reipurth, B., & Tokunaga, A., 2007, *AJ*, 133, 1528
- Connelley, M., Reipurth, B., & Tokunaga, A., 2008a, *AJ*, 135, 2496
- Connelley, M., Reipurth, B., & Tokunaga, A., 2008b, *AJ*, 135, 2526
- Connelley, M., & Greene, T., 2014, *AJ*, 147, 125
- Connelley, M.S., & Greene, T., 2010, *AJ*, 140, 1214
- Connelley, M.S., Reipurth, B., Tokunaga, A. 2007, *AJ*, 133, 1528
- Contreras, M.E., Sicilia-Aguilar, A., Muzerolle, J. et al., 2002, *AJ*, 124, 1585
- Contreras Peña, C., Lucas, P.W., Minniti, D. et al., 2017, *MNRAS*, 465, 3039
- Covino, E., Terranegra, A., Vittone, A., & Russo, G., 1984, *AJ*, 89, 1868
- Cushing, M., Vacca, W., & Rayner, J., 2004, *PASP*, 116, 362

- Dahm, S.E. 2008, in *Handbook of Star Forming Regions Vol. I*, Ed. Bo Reipurth, ASP, p. 966
- Dahm, S. & Hillenbrand, L.A. 2017, *AJ*, 154, A177
- Dame, T.M. & Thaddeus, P. 1985, *ApJ*, 297, 751
- Das, A., Das, H.S., Senorita Devi, A. 2015, *MNRAS*, 452, 389
- Devine, D., Reipurth, B., Bally, J. 1997, in *Low Mass Star Formation - from Infall to Outflow*, Poster proceedings of IAU Symposium No. 182, eds. F. Malbet & A. Castets, p. 91.
- Dobashi, K., Bernard, J.-P., Yonekura, Y., Fukui, Y. 1994, *ApJS*, 95, 419
- Doppmann, G., Greene, T., Covey, K., & Lada, C., 2005, *AJ*, 130, 1145
- Dunham, M., Arce, H., Bourke, T., et al., 2012, *ApJ*, 755, 157
- Dzib, S., Loinard, L., Mioduszewski, A.J. et al., 2010, *ApJ*, 718, 610
- Dzib, S., Loinard, L., Mioduszewski, A.J. et al., 2011, *Rev. Mex. AA Serie Conf.* 40, 231
- Eiroa, C. & Casali, M.M. 1992, *A&A*, 262, 468
- Elias, J., 1978, *ApJ*, 223, 859
- Evans, N.J., Balkum, S., Levreault, R.M., Hartmann, L., Kenyon, S.J., 1994, *ApJ*, 424, 793
- Fischer, W., Megeath, S. T., Tobin, J. J., et al., 2012, *ApJ*, 756, 99
- Fridlund, C.V.M. & Liseau, R. 1998, *ApJ*, 499, L75
- Fridlund, C.V.M., Nordh, H.L., van Duinen, R.J. et al., 1980, *A&A*, 91, L1
- Friesen, R.K., Bourke, T.L., Di Francesco, J. et al., 2016, *ApJ*, 833, A204
- Garrison, R.F. & Kormendy, J. 1976, *PASP*, 88, 865
- Goodrich, R.W. 1987, *PASP*, 99, 116
- Graham, J., & Frogel, J., 1985, *ApJ*, 289, 331
- Gramajo, L., Rodon, J., & Gomez, M., 2014, *AJ*, 147, 140
- Green, J.D., Kraus, A.L., Rizzuto, A.C. et al., 2016, *ApJ*, 830, A29
- Greene, T., & Lada, C., 1996, *AJ*, 112, 2184

- Greene, T.P., Aspin, C., Reipurth, B. 2008, *AJ*, 135, 1421
- Haas, M., Christou, J., Zinnecker, H., Ridgway, S., & Leinert, Ch., 1993, *A&A*, 269, 282
- Hackstein, M., Haas, M., Kóspál, A. et al., 2015, *A&A*, 582, L12
- Haro, G., 1953, *ApJ*, 117, 73
- Hartmann, L. & Kenyon, S.J. 1985, *ApJ*, 299, 462
- Hartmann, L. & Kenyon, S.J. 1987, *ApJ*, 322, 393
- Hartmann, L., & Kenyon, S., 1996, *ARA&A*, 34, 207
- Hartmann, L., Kenyon, S.J., Hewett, R. et al., 1989, *ApJ*, 338, 1001
- Harvey, P.M., Huard, T.L., Jørgensen, J.K. et al., 2008, *ApJ*, 680, 495
- Herbig, G., 1960, *ApJS*, 4, 337
- Herbig, G., 1966, *Vistas in Astronomy*, 8, 109
- Herbig, G., 1977, *ApJ*, 217, 693
- Herbig, G.H. 2007, *AJ*, 133, 2679
- Herbig, G.H. 2008, *AJ*, 135, 637
- Herbig, G.H. 2009, *AJ*, 138, 448
- Herbig, G.H., Petrov, P.P., Duemmler, R. 2003, *ApJ*, 595, 384
- Herbig, G.H. & Dahm, S.E. 2006, *AJ*, 131, 1530
- Herbig, G.H., & Harlan, E., 1971, *Information Bulletin of Variable Stars*, No. 543, Konkoly Obs., Budapest
- Herczeg, G.J., Dong, S., Shappee, B.J. et al., 2016, *ApJ*, 831, 133
- Hessman, F.V., Eislöffel, J., Mundt, R. et al., 1991, *ApJ*, 370, 384
- Hillenbrand, L., & Findeisen, K., 2015, *ApJ*, 808, 68
- Hodapp, 1999, *AJ*, 118, 1338
- Hodapp, K., Chini, R., Waterman, R., Lemke, R., 2012, *ApJ*, 744, 56

- Hosokawa, T., Offner, S.R., Krumholz, M.R. 2011, *ApJ*, 738, A140
- Jeffries, R.D. 2007, *MNRAS*, 376, 1109
- Jurdana-Sepic, R. & Munari, U. 2016, *New Astron.*, 43, 873
- Kaltcheva, N., Hilditch, R., 2000, *MNRAS*, 312, 753
- Kamezaki, T., Imura, K., Omodaka, T. et al., 2014, *ApJS*, 211, A18
- Kenyon, S.J., Hartmann, L., Hewett, R. 1988, *ApJ*, 325, 231
- Kenyon, S., Hartmann, L., & Kolotilov, E., 1991, *PASP*, 103, 1069
- Kenyon, S.J., Hartmann, L., Gomez, M., Carr, J.S. 1993, *AJ*, 105, 1505
- Khanzadyan, T., Davis, C.J., Aspin, C. et al., 2012, *A&A*, 542, A111
- Kim, B.G., Kawamura, A., Yonekura, Y., Fukui, Y. 2004, *PASJ*, 56, 313
- Kopatskaya, E.N., Kolotilov, E.A., Arkharov, A.A. 2013, *MNRAS*, 434, 38
- Kóspál, A., Ábrahám, P., Prusti, T. et al., 2007, *A&A*, 470, 211
- Kóspál, A., Ábrahám, P., Apai, D., et al., 2008, *MNRAS*, 383, 1015
- Kóspál, A., Ábrahám, P., Moór, A. et al., 2015, *ApJ*, 801, L5
- Kóspál, A., Ábrahám, P., Acosta-Pulido, J.A. et al. 2016, *A&A*, 596, A52
- Kóspál, A., Ábrahám, P., Westhues, Ch., Haas, M., 2017, *A&A*, 597, L10
- Kounkel, M., Hartmann, L., Loinard, L. et al., 2017, *ApJ*, 834, A142
- Kraus, S., Caratti o Garatti, A., Garcia-Lopez, R., Kreplin, A., Aarnio, A., Monnier, J., Naylor, T., Weigelt, G., 2016, *MNRAS*, 462L, 61K
- Kun, M. 1998, *ApJS*, 115, 59
- Kun, M. 2008, in *Handbook of Star Forming Regions Vol. I*, ed. Bo Reipurth, ASP, p.240
- Kun, M., Kiss, Z.T., Balog, Z. 2008, in *Handbook of Star Forming Regions Vol. I*, ed. Bo Reipurth, ASP, p.136
- Kun, M., Szegedi-Elek, E., Reipurth, B. 2017, *MNRAS*, 468, 2325
- Lada, C.J., Alves, J., Lada, E.A. 1999, *ApJ*, 512, 250

- Lada, C.J., Lombardi, M., Alves, J.F. 2009, *ApJ*, 703, 52
- Larson, R.B. 1980, *MNRAS*, 190, 321
- Laugalys, V., Straizys, V., Vrba, F.J. et al., 2006, *Baltic Astron.*, 15, 483
- Lim, J., Yeung, P.K.H., Hanawa, T. et al., 2016, *ApJ*, 826, A153
- Loinard, L., Torres, R.M., Mioduszewski, A.J. et al., 2007, *ApJ*, 671, 546
- Maehara, H., Kojima, T., & Fujii, M., 2014, *ATel*, 6770
- Magakian, T.Yu., Nikogossian, E.H., Aspin, C. et al., 2010, *AJ*, 139, 969
- Magakian, T., Nikogossian, E. H., Movsessian, T., et al., 2013, *MNRAS*, 432, 2685
- Massi, F., Codella, C., Brand, J., di Fabrizio, L., & Wouterloot, J., 2008, *A&A*, 490, 107
- Mayne, N.J. & Naylor, T., 2008, *MNRAS*, 386, 261
- McNeil, J., Reipurth, B., & Meech, K., 2004, *IAUC* 8284
- Miller, A., Hillenbrand, L.A., Covey, K.R. et al., 2011, *ApJ*, 730, 80
- Mould, J.R., Hall, D.N.B., Ridgway, S.T. et al., 1978, *ApJ*, 222, L123
- Movsessian, T., Khanzadyan, T., Aspin, C. et al., 2006, *A&A*, 455, 1001
- Munari, U., Milani, A., Valisa, P., & Semkov, E., 2010, *Atel*, 2808
- Mundt, R., Stocke, J., Strom, S., Strom, K., & Anderson, E., 1985, *ApJ*, 297, 41
- Murdin, P. & Penston, M.V. 1977, *MNRAS*, 181, 657
- Ortiz-León, G.N., Dzib, S.A., Kounkel, M.A. et al., 2017, *ApJ*, 834, A143
- Padoan, P. & Nordlund, A. 2004, *ApJ*, 617, 559
- Parsamian E. S., Petrossian V. M., 1979, *Akad. Nauk. Armenian SSR, Soobschenia*, No. 135, Yerevan
- Peneva, S., Semkov, E., Munari, U., & Birkle, K., 2010, *A&A*, 515, 24
- Perez, L.M., Lamb, J.W., Woody, D.P. et al., 2010, *ApJ*, 724, 493
- Persi, P., Ferrari-Toniolo, M., Busso, M., et al., 1988, *AJ*, 95, 1167

- Persson, R., 2004, IAU Circ, 8441
- Petrov, P.P. & Herbig, G.H. 1992, ApJ, 392, 209
- Petrov, P.P. & Herbig, G.H. 2008, 136, 676
- Petrov, P.P., Kurosawa, R., Romanova, M.M. et al., 2014, MNRAS, 442,3643
- Pfalzner, S. 2008, A&A, 492, 735
- Pickering, E., 1890, Ann. Harvard College Obs, 18, 113
- Poetzels, R., Mundt, R., & Ray, T., 1989, A&A, 224, L13
- Principe, D.A., Cieza, L., Hales, A. et al., 2018, MNRAS, 473, 879
- Prusti, T., Bontekoe, Tj., Chiar, J., Kester, D., & Whittet, D., 1993, A&A, 279, 163
- Pueyo, L., Hillenbrand, L., Vasisht, G., et al., 2012, ApJ, 757, 57
- Racine, R. 1968, AJ, 73, 233
- Rayner, J., Toomey, D., Onaka, P., et al., 2003, PASP, 15, 362
- Rayner, J., Cushing, M., & Vacca, W., 2009, ApJS, 185, 289
- M.J. Reid et al., 2014, ApJ, 783, 130
- Reipurth, B. 1985a, A&A, 143, 435
- Reipurth, B., 1985b, in *ESO/IRAM/ONSALA Workshop on (Sub)-Millimeter Astronomy*, ed. P. Shaver & K. Kj ar (Garching: ESO), p. 459
- Reipurth, B. 1990, in IAU Symp. No. 137 *Flare stars in star clusters, associations and the solar vicinity*, Kluwer, p. 229
- Reipurth, B. 2016, *George Herbig and Early Stellar Evolution*, <http://ifa.hawaii.edu/SP1>
- Reipurth, B., & Aspin, C., 1997, AJ, 114, 2700
- Reipurth, B. & Aspin, C. 2004a, ApJ, 608, L65
- Reipurth, B. & Aspin, C., 2004b, ApJ, 606, L119

- Reipurth, B. & Aspin, C. 2010, in Victor Ambartsumian Centennial Volume "Evolution of Cosmic Objects through their Physical Activity", eds. Hayk Harutyunyan, Areg Mickaelian and Yervant Terzian, Gitutyun Publishing House, Yerevan, Armenia, p. 19
- Reipurth, B. & Bally, J. 1986, *Nature*, 320, 336
- Reipurth, B. & Clarke, C.J. 2001, *AJ*, 122, 432
- Reipurth, B., Bally, J., & Devine, D., 1997a, *AJ*, 114, 2708
- Reipurth, B., Olberg, M., Gredel, R., & Booth, R., 1997b, *A&A*, 327, 1164
- Reipurth, B., Hartmann, L., Kenyon, S., Smette, A., & Bouchet, P., 2002, *AJ*, 124, 2194
- Reipurth, B., Aspin, C., Beck, T., et al., 2007, *AJ*, 133, 1000
- Reipurth, B., Aspin, C., & Herbig, G., 2012, *ApJ*, 748, L5
- Rodriguez, L.F., Porras, A., Claussen, M.J. et al., 2003, *ApJ*, 586, L137
- Samus, N., 2009, *CBET*, 1896, 1
- Sandell, G., & Aspin, C., 1998, *A&A*, 333, 1016
- Sandell, G. & Weintraub, D.A. 2001, *ApJS*, 134, 115
- Sandstrom, K.M., Peek, J.E.G., Bower, G.C. et al., 2007, *ApJ*, 667, 1161
- Schoonenberg, D., Okuzumi, S., Ormel, C.W. 2017, *A&A*, 605, L2
- Semkov, E., & Peneva, S., 2010, *IAU Inform. Bull. of Variable Stars*, No. 5939
- Semkov, E., Peneva, S., Munari, U., Milani, A., & Valisa, P., 2010, *A&A*, 523, L3
- Semkov, E., Peneva, S.P., Munari, U., 2012, *A&A*, 542, 43
- Semkov, E., Peneva, S.P., Munari, U., 2013, *A&A*, 556, 60
- Simons, D., & Tokunaga, A., 2002, *PASP*, 114, 169
- Skinner, S.L., Sokal, K.R., Güdel, M., Briggs, K.R. 2009, *ApJ*, 696, 766
- Smith R. G., 1993, *MNRAS*, 264, 587
- Staude, H., & Neckel, Th., 1991, *A&A*, 244, L13

- Staude, H., & Neckel, Th., 1992, *ApJ*, 400, 556
- Stocke, J., Hartigan, P., Strom, S., et al., 1988, *ApJS*, 68, 229
- Straizys, V., Cernis, K., Bartasiute, S. 1996, *Balt. Astr.* 5, 125
- Strom, K., & Strom, S., 1993, *ApJ*, 412, L63
- Testi, L., Natta, A., Scholz, A. et al., 2016, *A&A*, 593, A111
- Thommes, J., Reipurth, B., Aspin, C., & Herbig, G., 2011, *CBET*, No. 2795
- Tobin, J.J., Chandler, C.J., Wilner, D.J. et al., 2013, *ApJ*, 779, A93
- Tokunaga, A., & Simons, D., 2002, *PASP*, 114, 180
- Turner, D.G. 2012, *Astron. Nach.* 333, 174
- Vacca, W., Cushing, M., & Simon, T., 2004, *ApJ*, 609, L29
- Varricatt, W.P., Kerr, T.H., Carroll, T., Moore, E. 2015, *ATel* 8174
- Velazquez, P.F. & Rodriguez, L.F. 2001, *Rev. Mex. Astron. Astrofis.*, 37, 261
- Vorobyov, E.I. & Basu, S. 2015, *ApJ*, 805, A115
- Wachmann, A., 1954, *ZfA*, 35, 74
- Wang, H., Apai, D., Henning, T., & Pascucci, I., *ApJ*, 601, L83
- Walker, M., 1959, *ApJ*, 130, 57
- Welin, G., 1971a, *Information Bulletin on Variable Stars*, No. 581
- Welin, G., 1971b, *A&A*, 12, 312
- Welin, G. 1976, *A&A*, 49, 145
- Welty, A.D., Strom, S.E., Edwards, S. et al., 1992, *ApJ*, 397, 260
- Whelan, E.T., Dougados, C., Perrin, M.D. et al., 2010, *ApJ*, 720, L119
- Whitworth, A.P. & Zinnecker, H. 2004, *A&A*, 427, 299
- Wolstencroft, R.D., Scarrott, S.M., Warren-Smith, R.F. et al., 1986, *MNRAS*, 218, 1P
- Zhu, Z., Hartmann, L., Calvet, N. et al., 2007, *ApJ*, 669, 483

Zhu, Z., Hartmann, L., Calvet, N., et al., 2008, ApJ, 684, 1281

Zhu, Z., Hartmann, L., Gammie, C., McKinney, J. 2009, ApJ, 701, 620

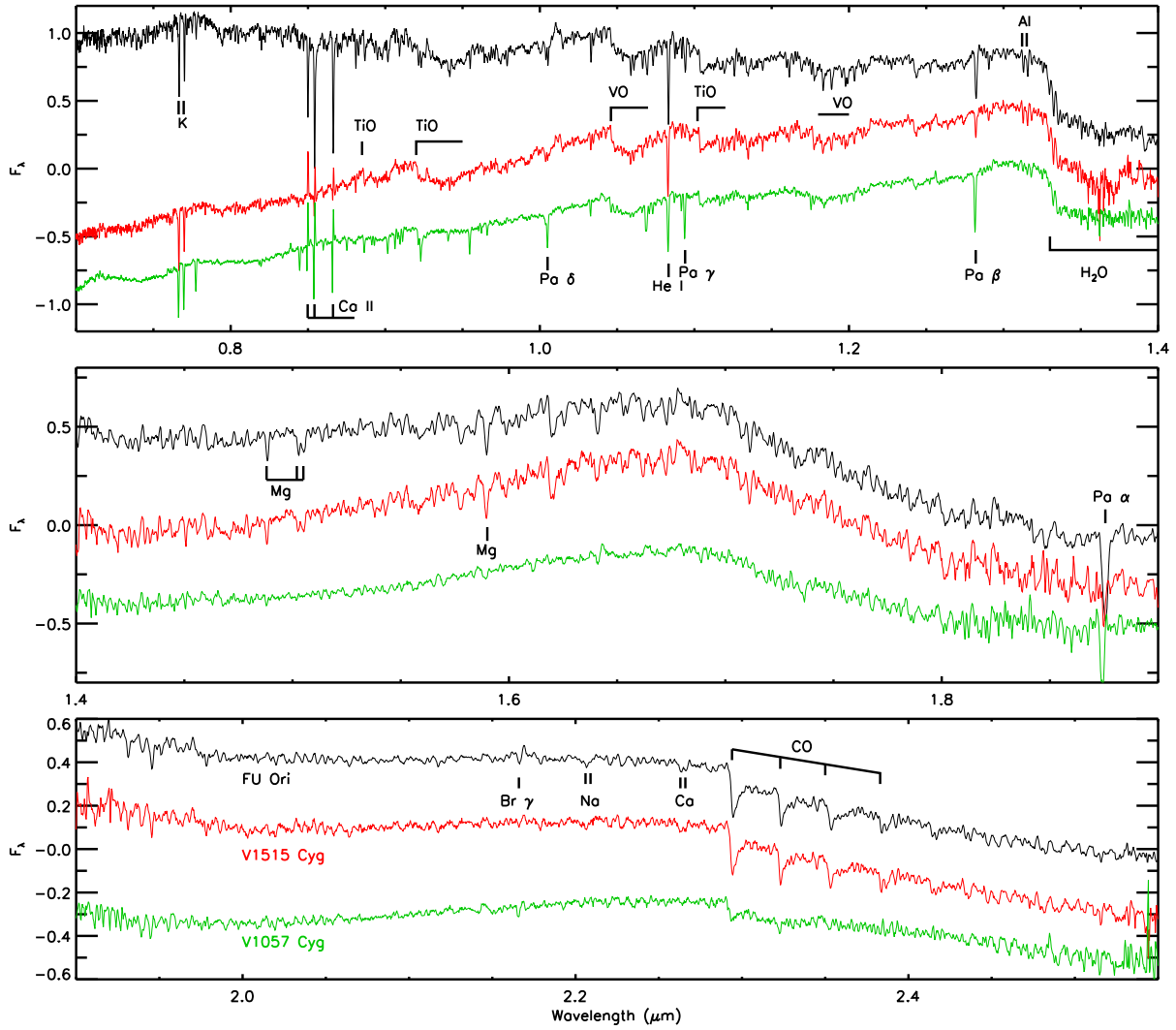


Fig. 1.— J, H, and K-band spectra of the three classical FUors discussed by Herbig (1977): FU Ori (black), V1515 Cyg (red), and V1057 Cyg (green).

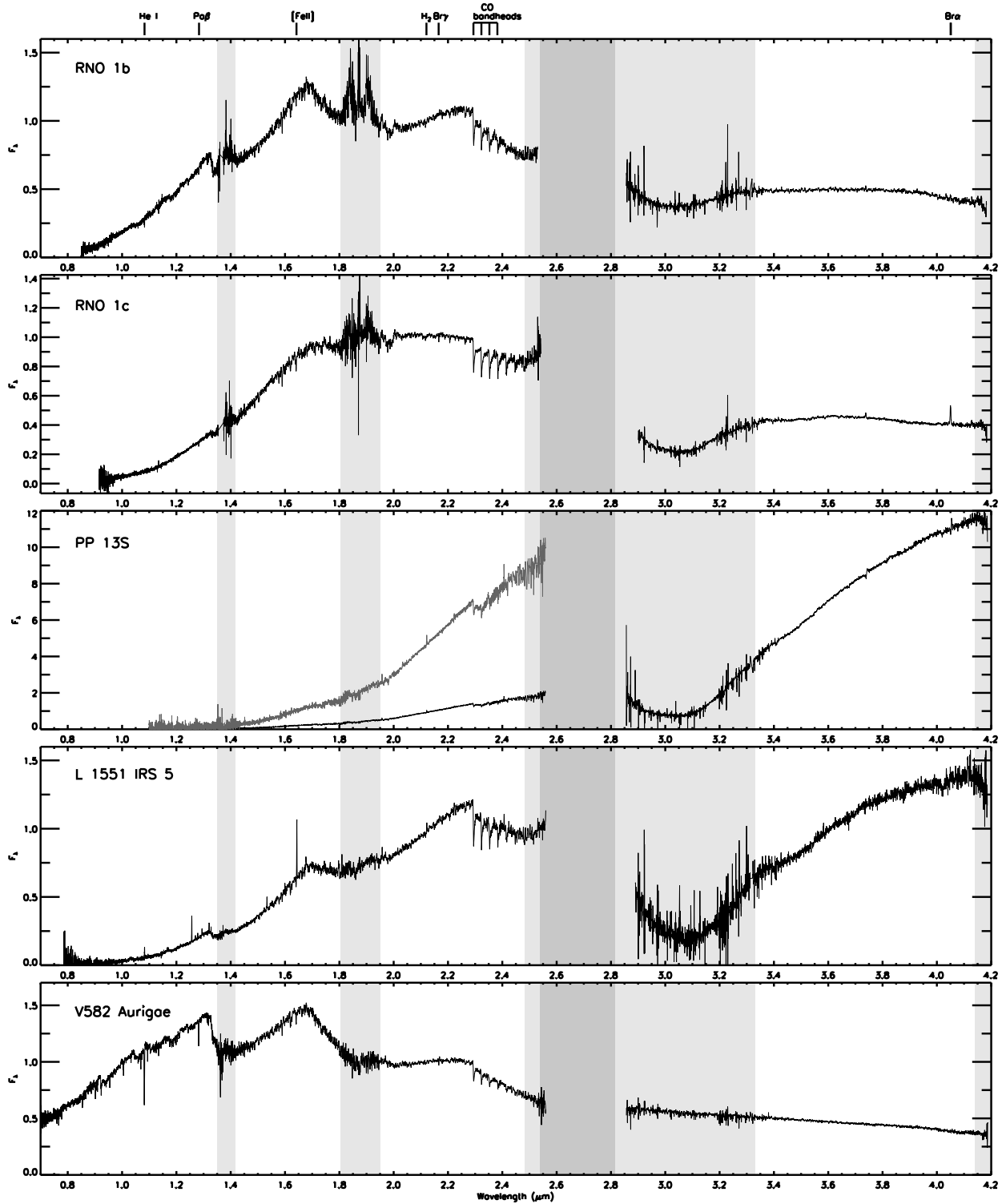


Fig. 2.— An atlas of 33 objects each of which have been suggested in the literature to be related to the FUor phenomenon. The light gray regions show areas of strong telluric absorption, and the darker gray area shows where the atmosphere is quite opaque. For PP 13 S, the 1-2.5 μm spectrum has been overplotted in dark gray rescaled by a factor of 5 to better show the features in this part of the spectrum.

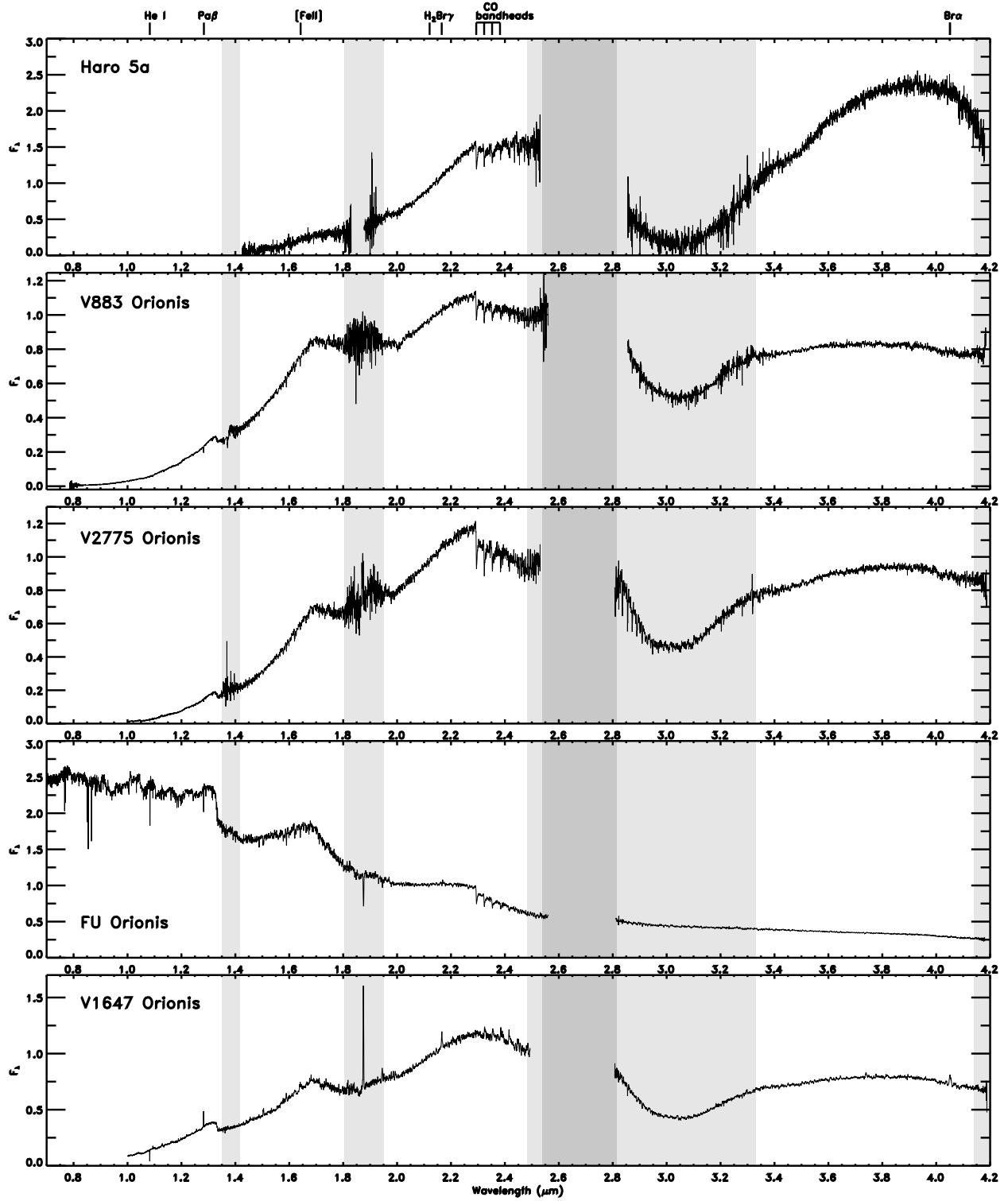


Fig. 2.— continued

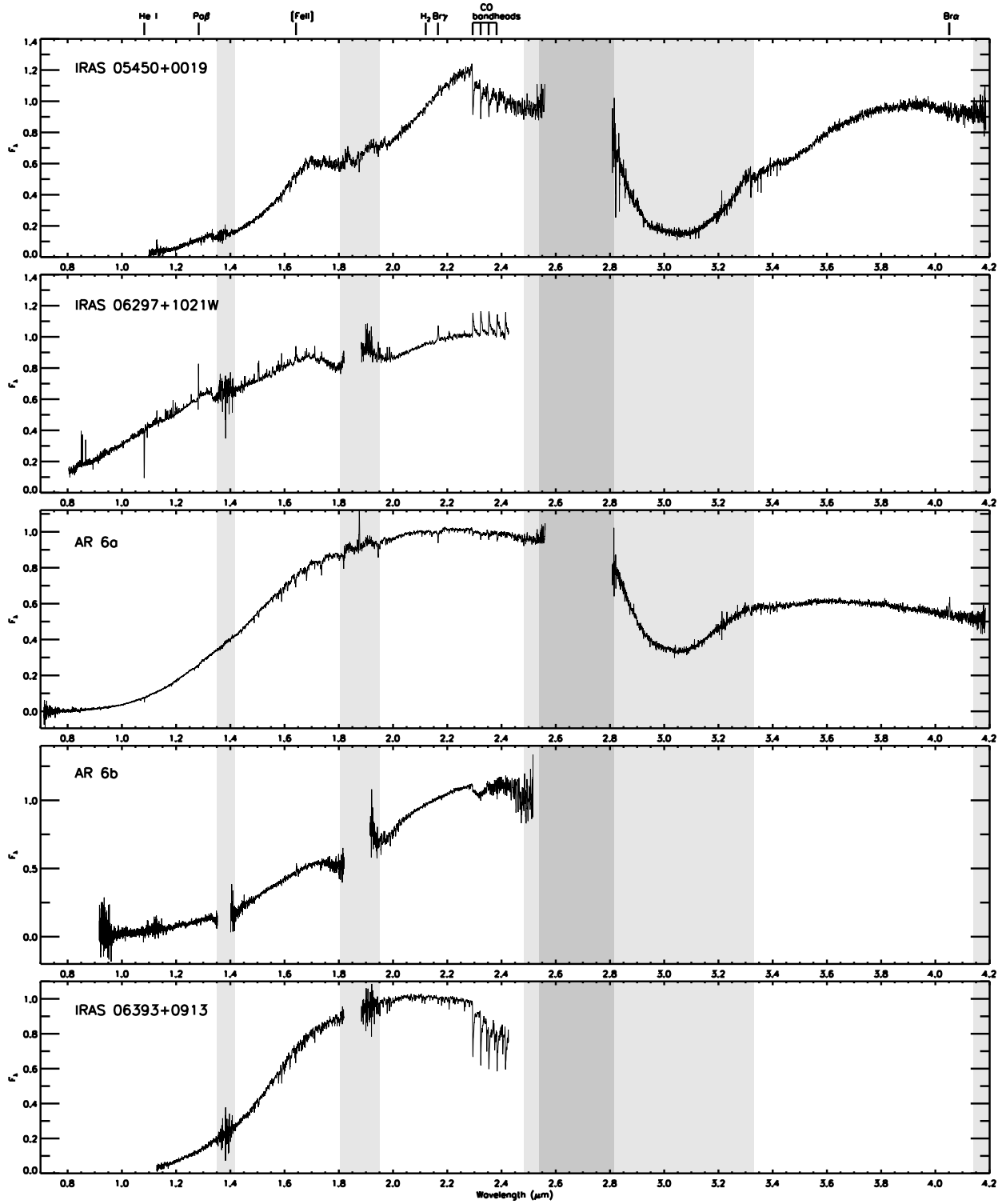


Fig. 2.— continued

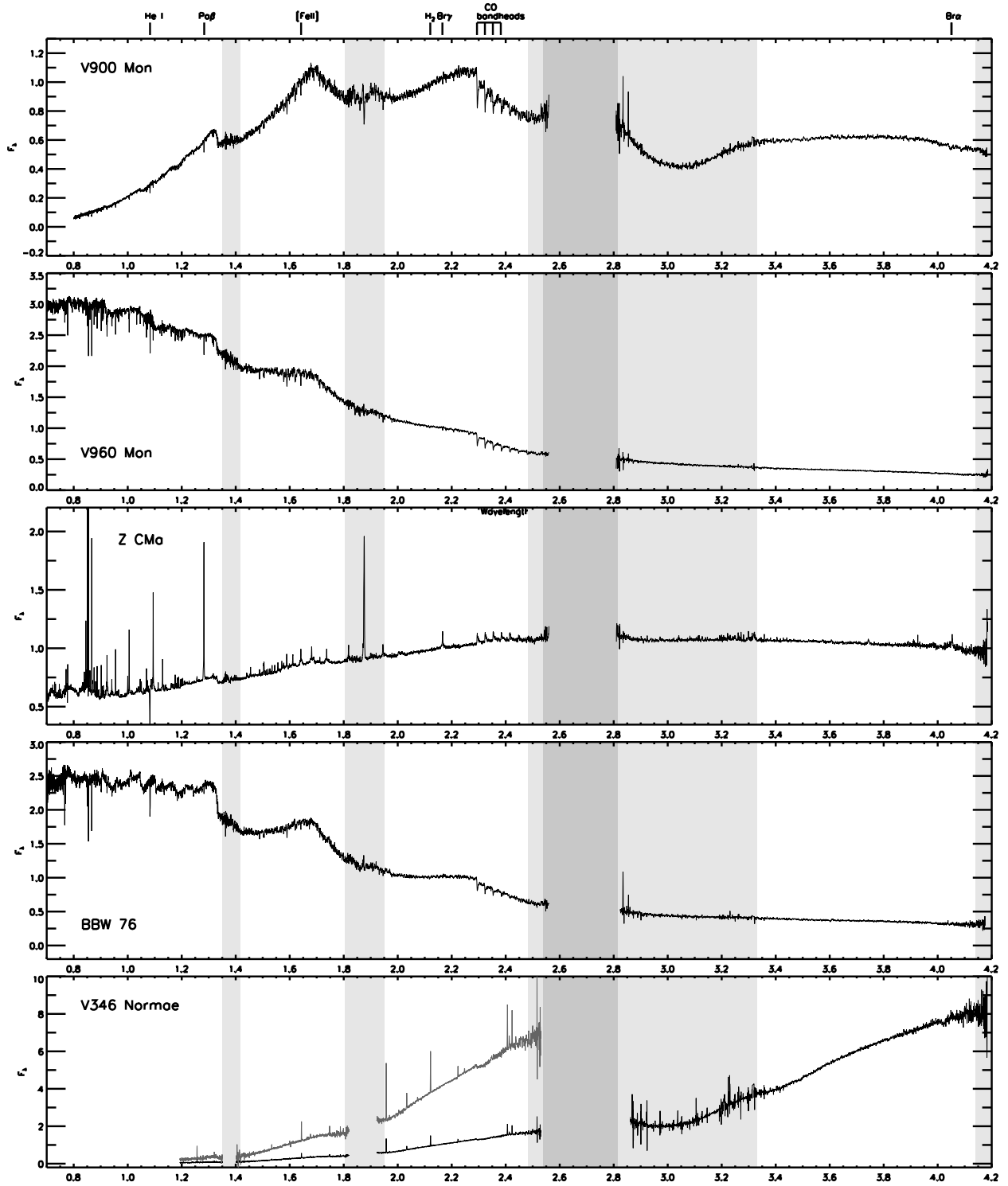


Fig. 2.— . For V346 Normae, the 1-2.5 μm spectrum that has been overplotted in dark gray was scaled by a factor of 4 to better show the features in this part of the spectrum.

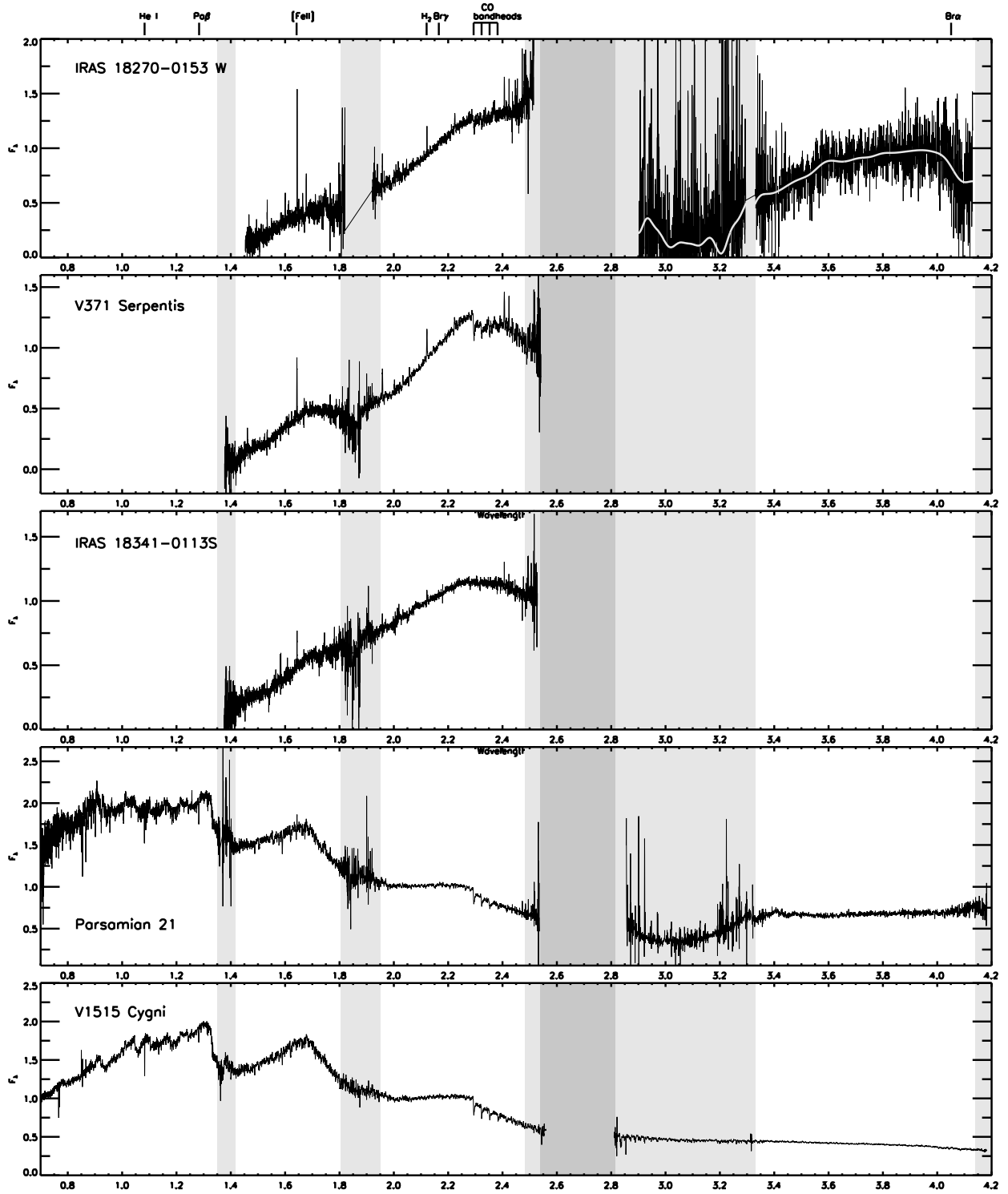


Fig. 2.— The white line through the L-band portion of the spectrum of IRAS 18270-0153W has been boxcar smoothed to better show the overall shape of the spectrum in this region.

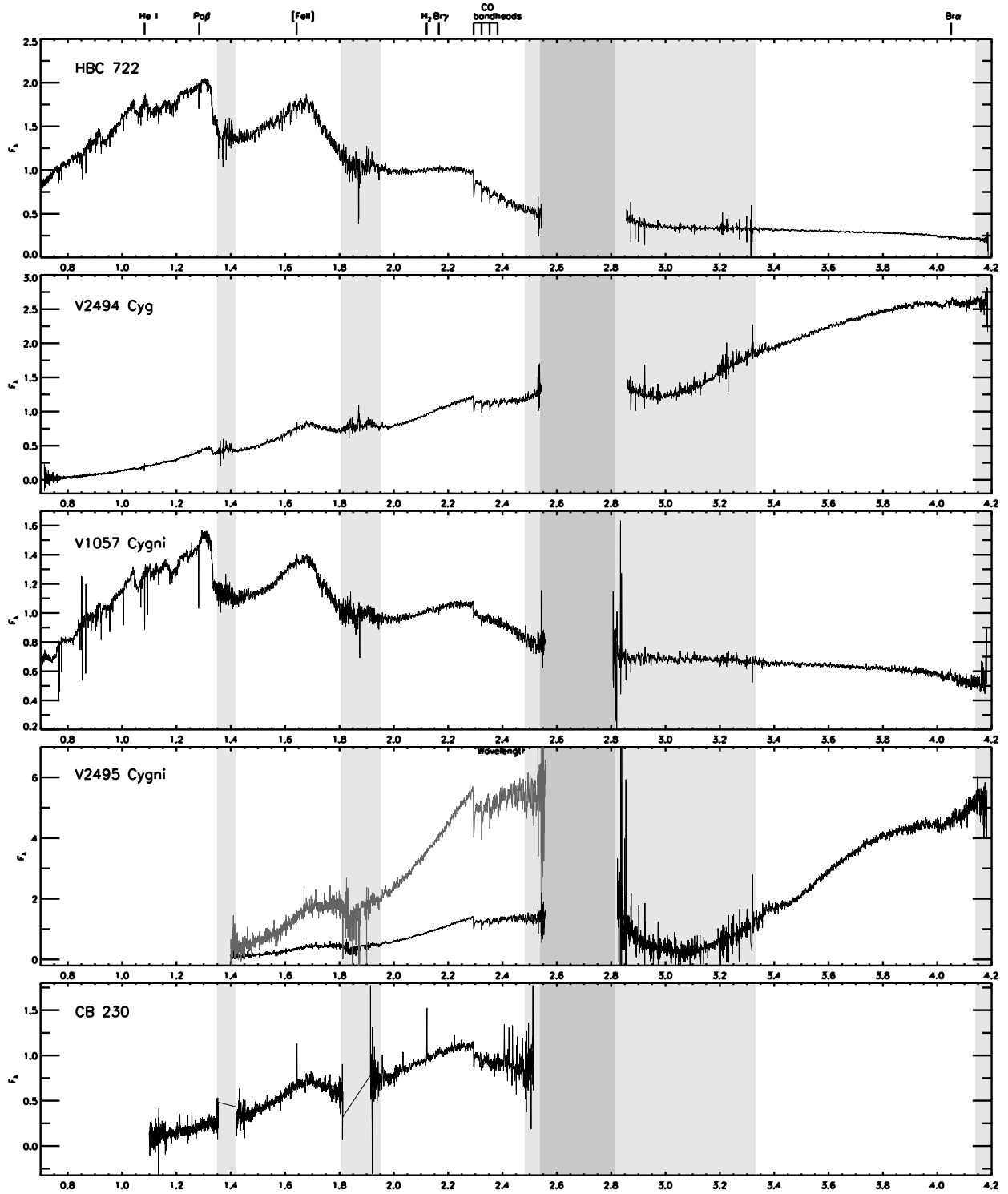


Fig. 2.— For V2495 Cygni, the 1-2.5 μm spectrum that has been overplotted in dark gray was scaled by a factor of 4 to better show the features in this part of the spectrum.

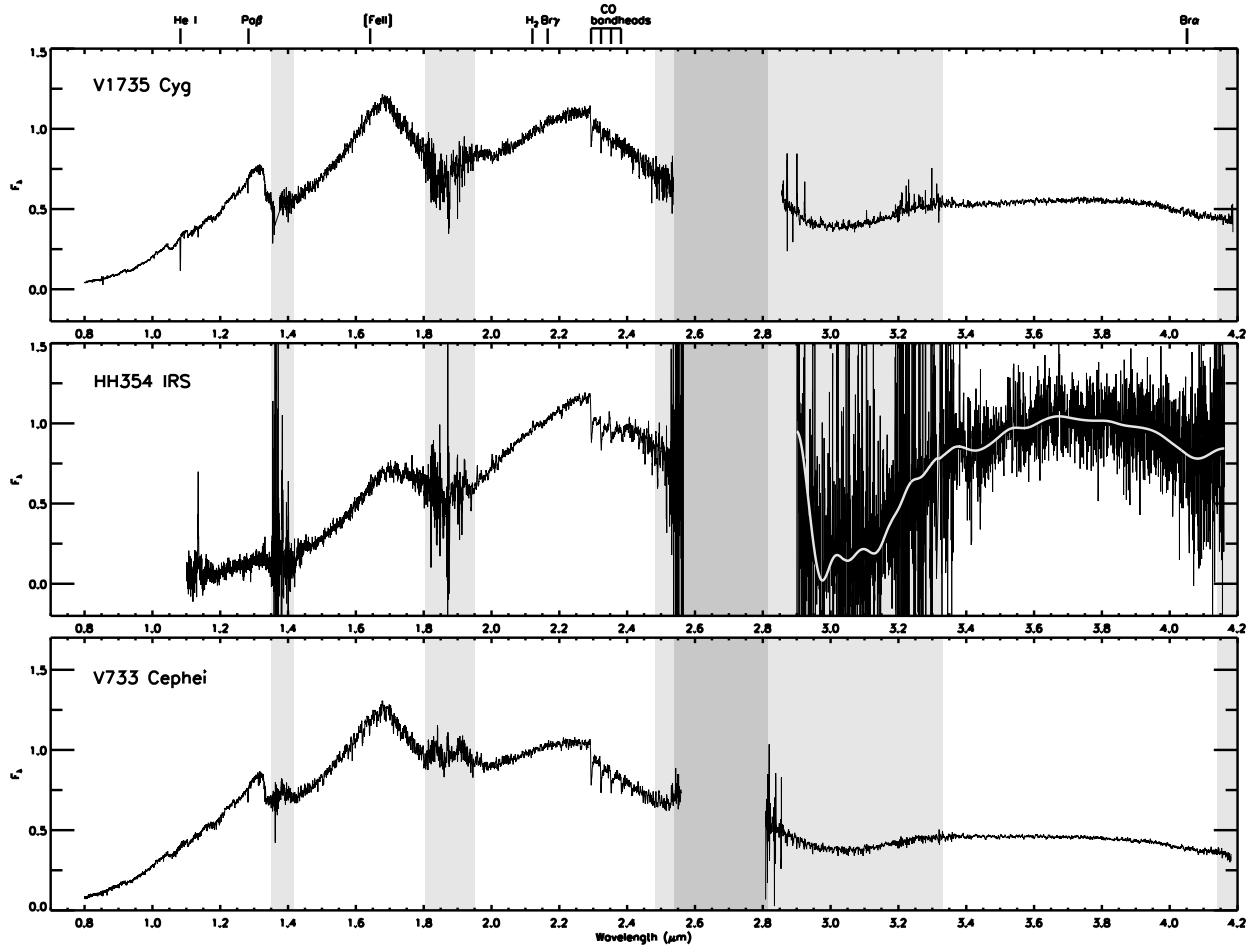


Fig. 2.— A smoothed spectrum of HH 354 IRS has been overlaid on the 3 to 4 μm region using a Gaussian kernel with a 0.02 μm standard deviation.

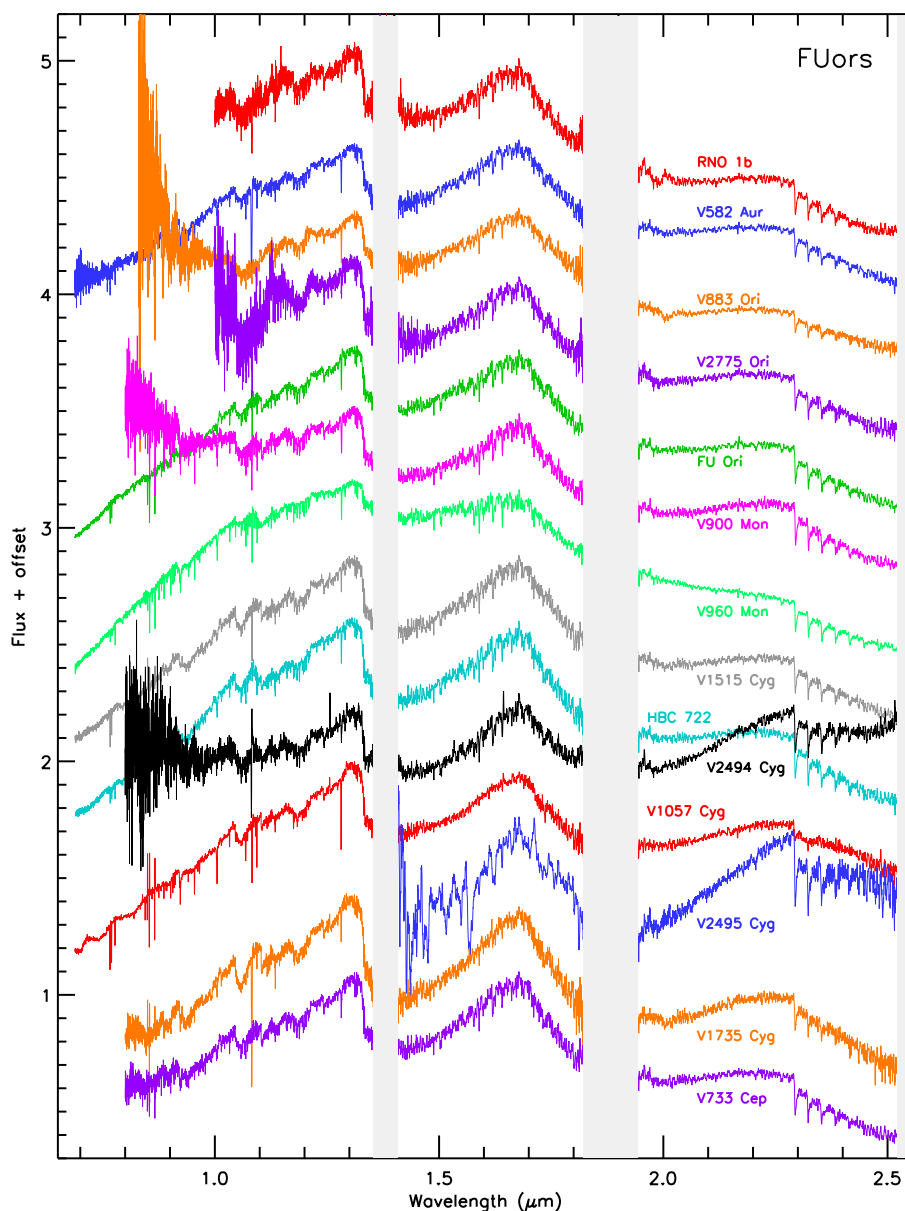


Fig. 3.— 0.7 μm to 2.5 μm spectra of only those FUors whose outburst was observed, with extinction added or removed to minimize the overall spectral slope. The common spectral features thus become apparent: strong He I absorption at 1.08 μm , a strong break at 1.32 μm and a 'triangular' H-band continuum due to water vapor absorption and low gravity, strong CO band heads starting at 2.29 μm , and weak metal absorption lines if any. $\text{Pa}\beta$ at 1.28 μm is also seen in absorption. The flux of each spectrum has been normalized at 2.15 μm , then offset.

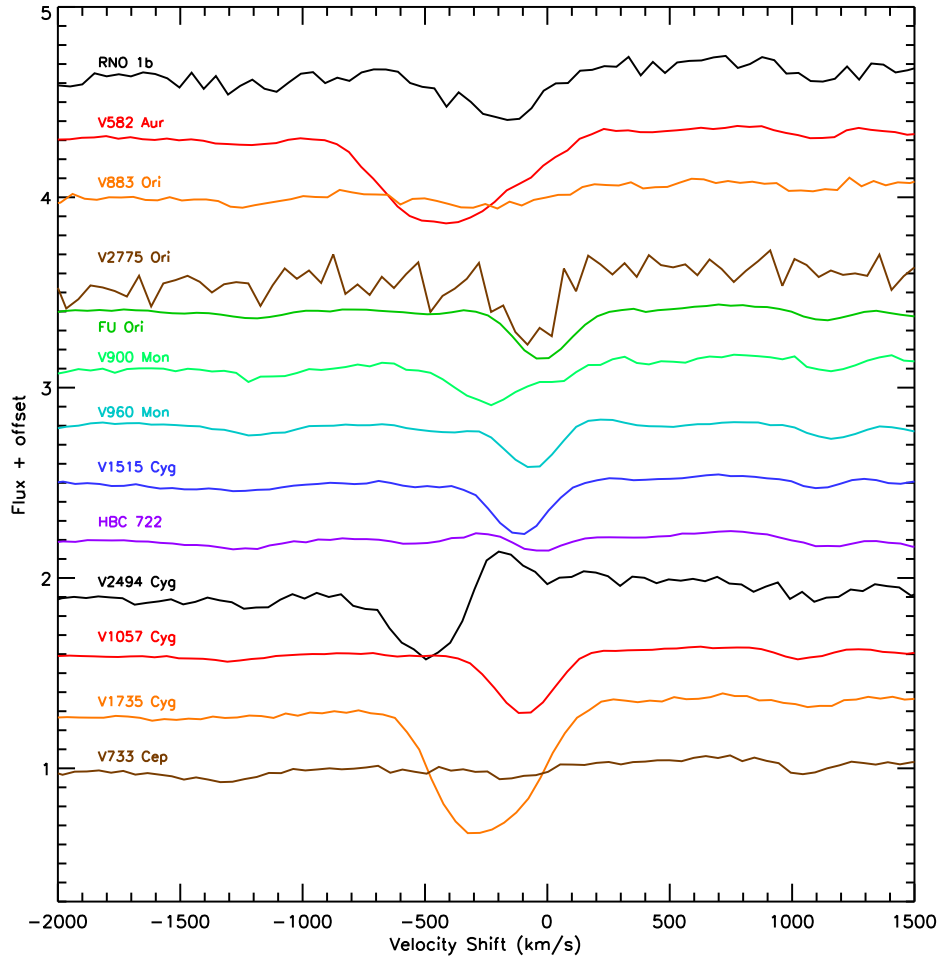


Fig. 4.— The He I λ 1.08 μm line profile, for only bona fide FUors. Nearly all of these lines show blue shifted absorption, with a mean velocity of $\sim 350 \text{ km s}^{-1}$.

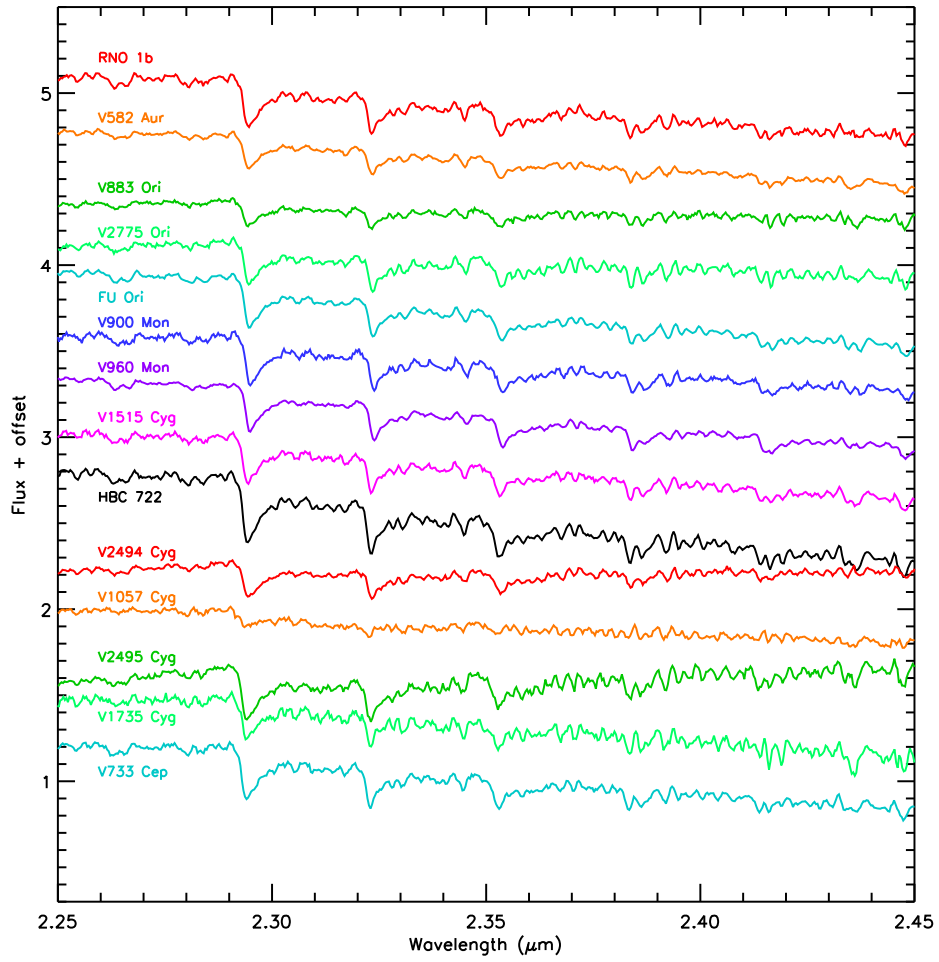


Fig. 5.— The CO band heads, for only bona fide FUors.

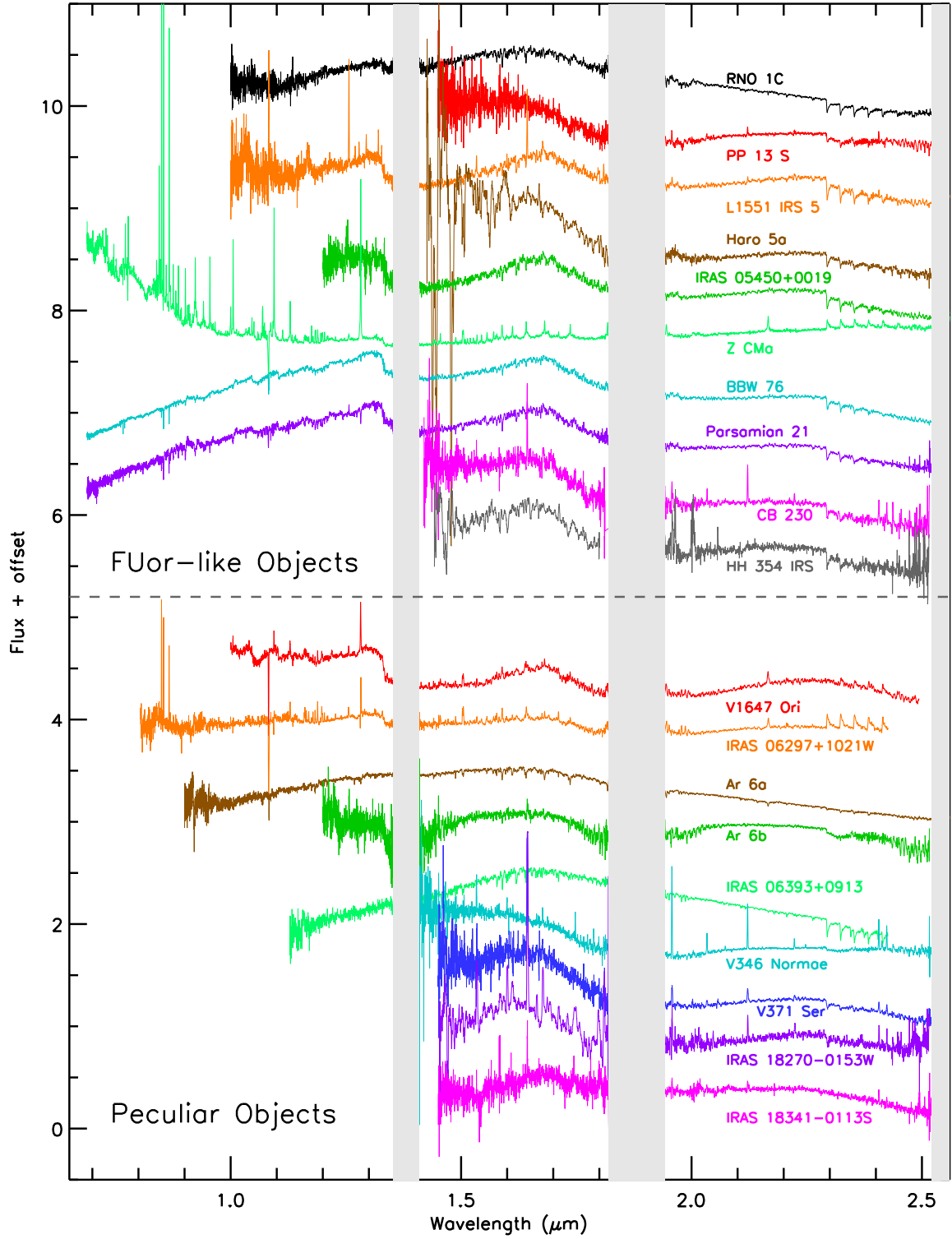


Fig. 6.— Same as for Figure 3, but for FUor-like objects (upper part) and peculiar objects with some FUor characteristics (lower part).

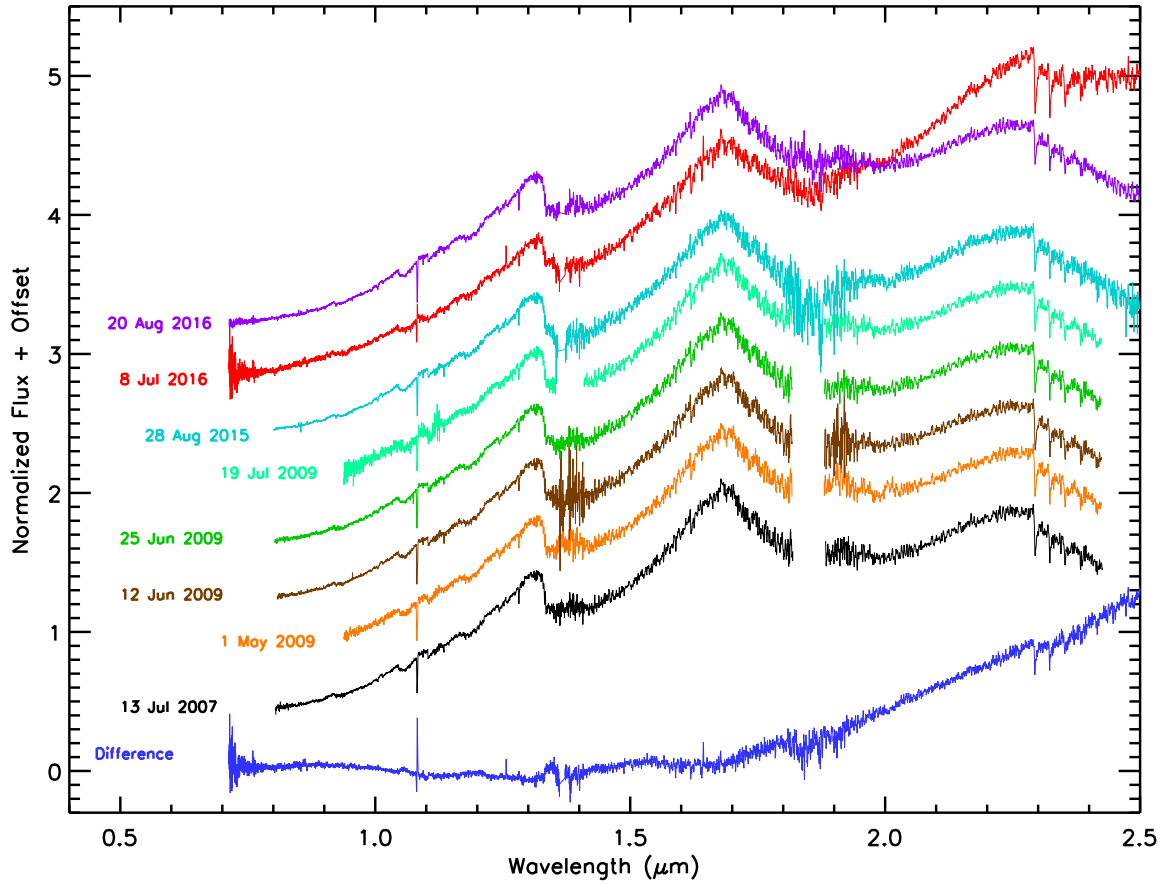


Fig. 7.— V1735 Cyg briefly showed unexpected spectroscopic variability in July 2016, then returned to its nominal state when next observed the following month. The difference between the July 2016 and August 2016 spectra is shown at the bottom. We see the addition of a featureless red continuum, but with additional CO absorption.

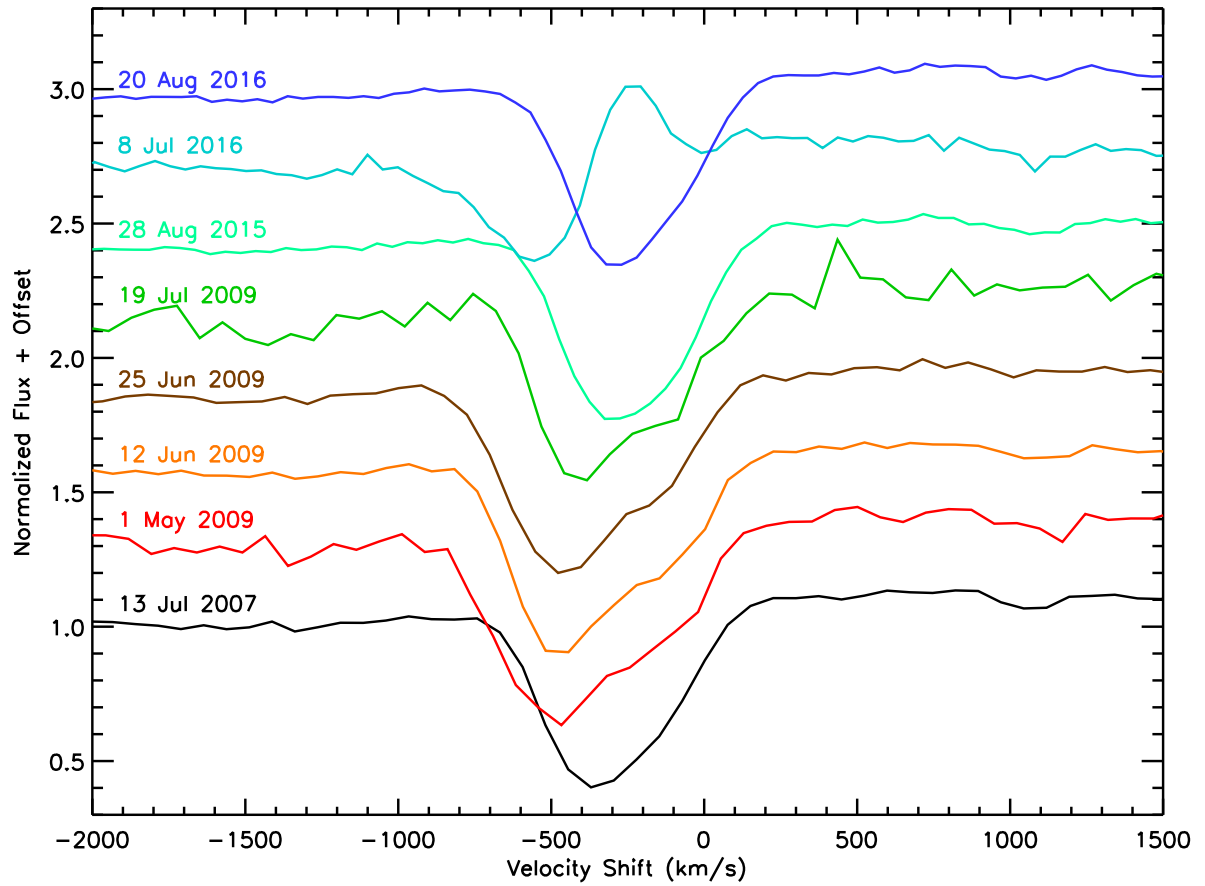


Fig. 8.— The He I λ 1.08 μm line for V1735 Cyg also showed blue shifted emission and faster blueshifted absorption with a velocity of $\sim 950 \text{ km s}^{-1}$ when its spectrum changed during the July 2016 event.

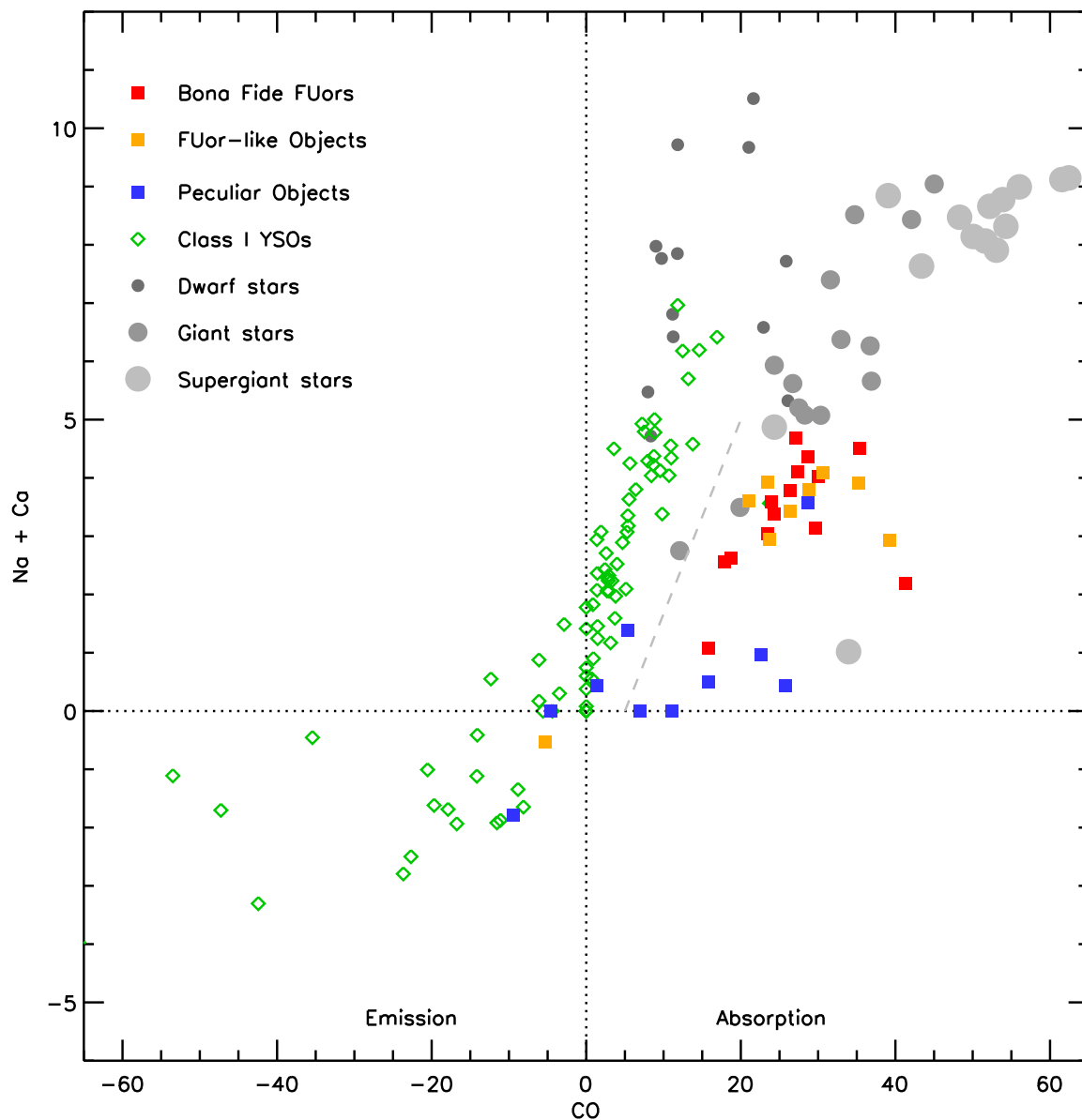


Fig. 9.— In a plot of the equivalent width (EW) of CO vs the EW of Na+Ca, FUors and FUor-like objects lie in a unique part of this space without significant overlap with field stars or other YSOs. The peculiar objects tend to be located closer to (0,0). Field M-stars from the SpeX library, shown as gray circles, are to the upper right. The dotted lines separate the regions of absorption and emission in the figure. A gray dashed line separates the FUors from the rest of the YSOs. If x is the EW of Na+Ca, then the CO EW is greater than $3x + 5$.

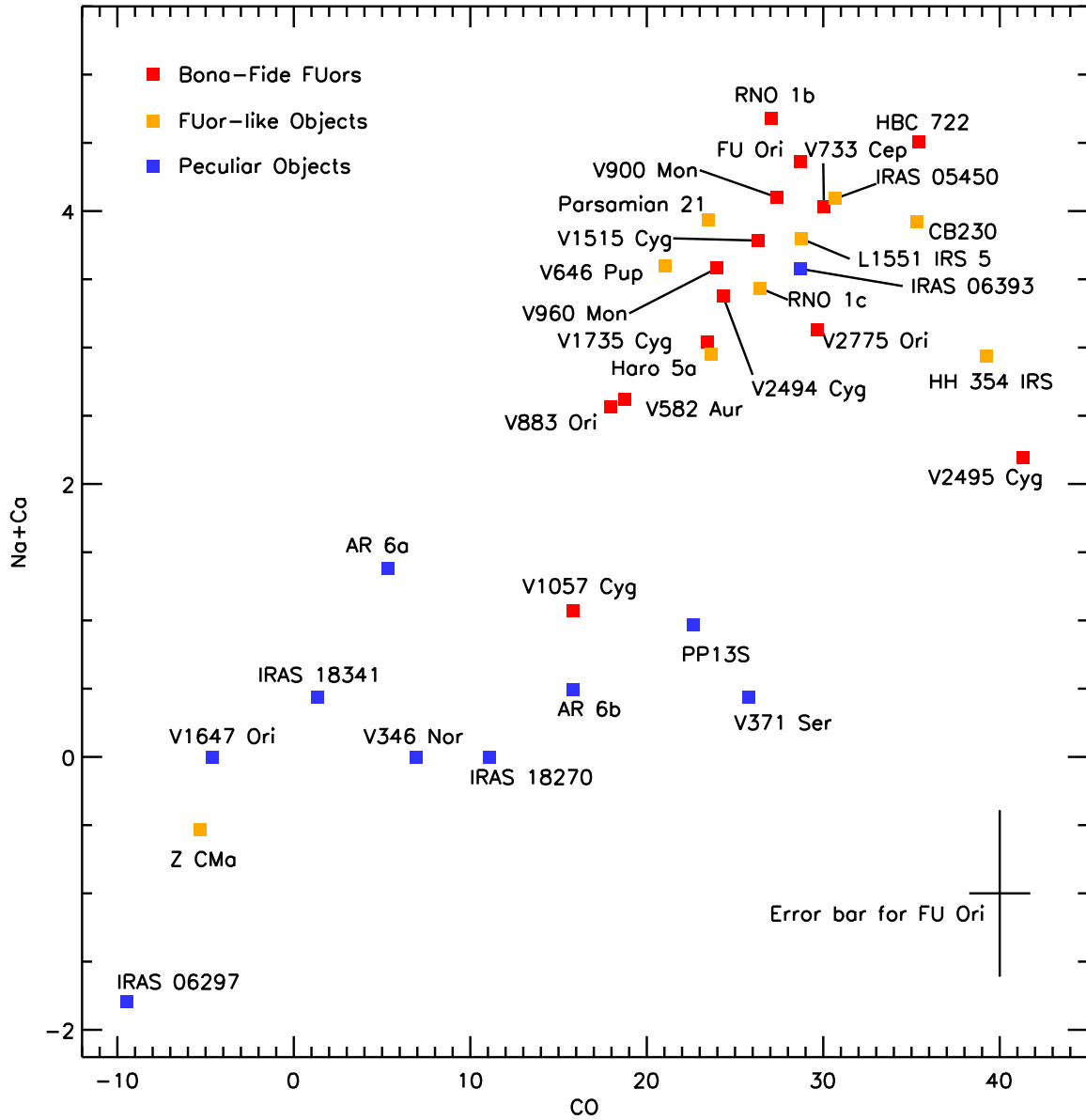


Fig. 10.— An enlargement of the previous figure showing the region of FUors, FUor-like objects, and peculiar objects, with identifications.

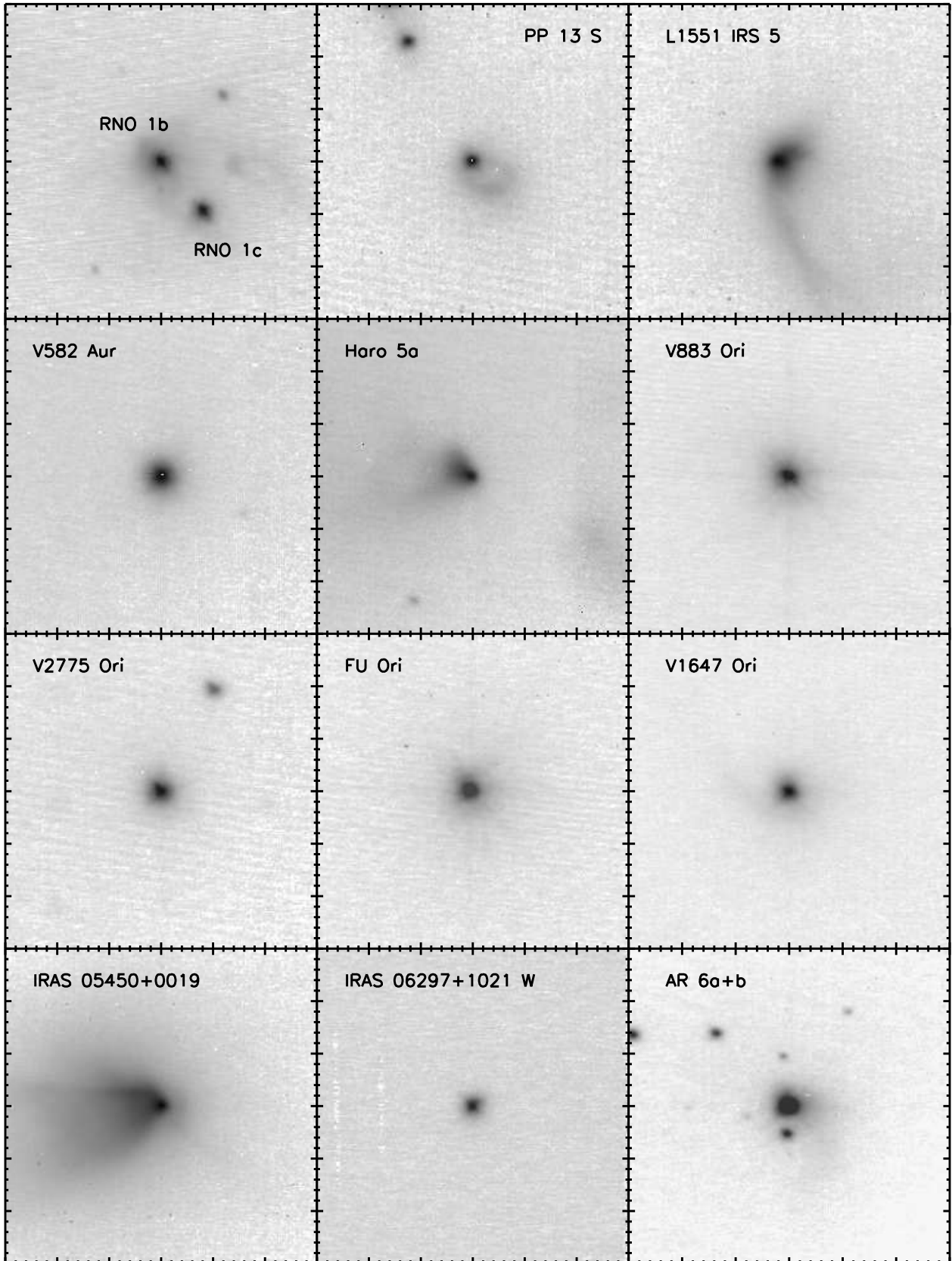


Fig. 11.— 30'' K-band images of our targets.

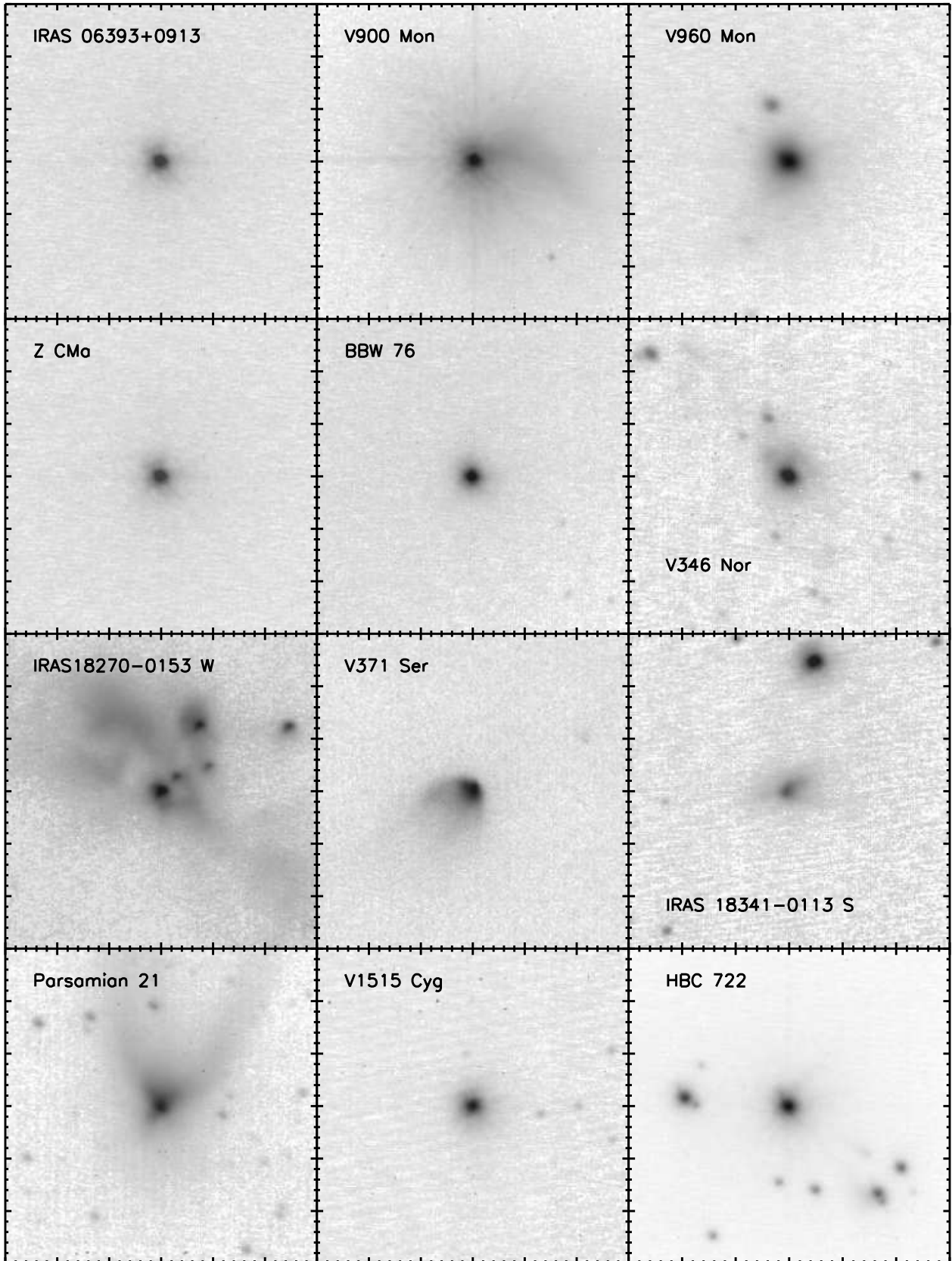


Fig. 11.— Continued

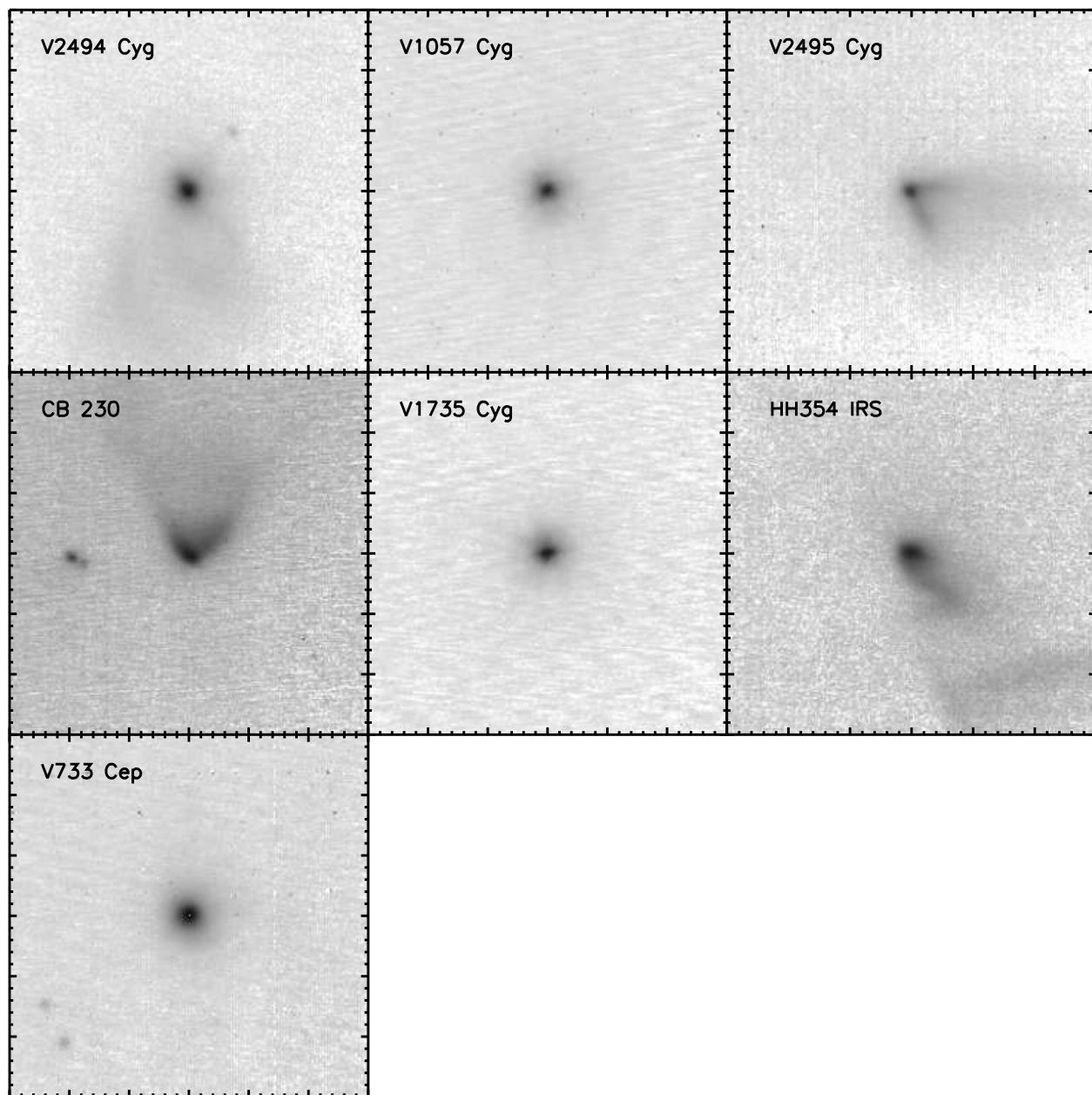


Fig. 11.— Continued

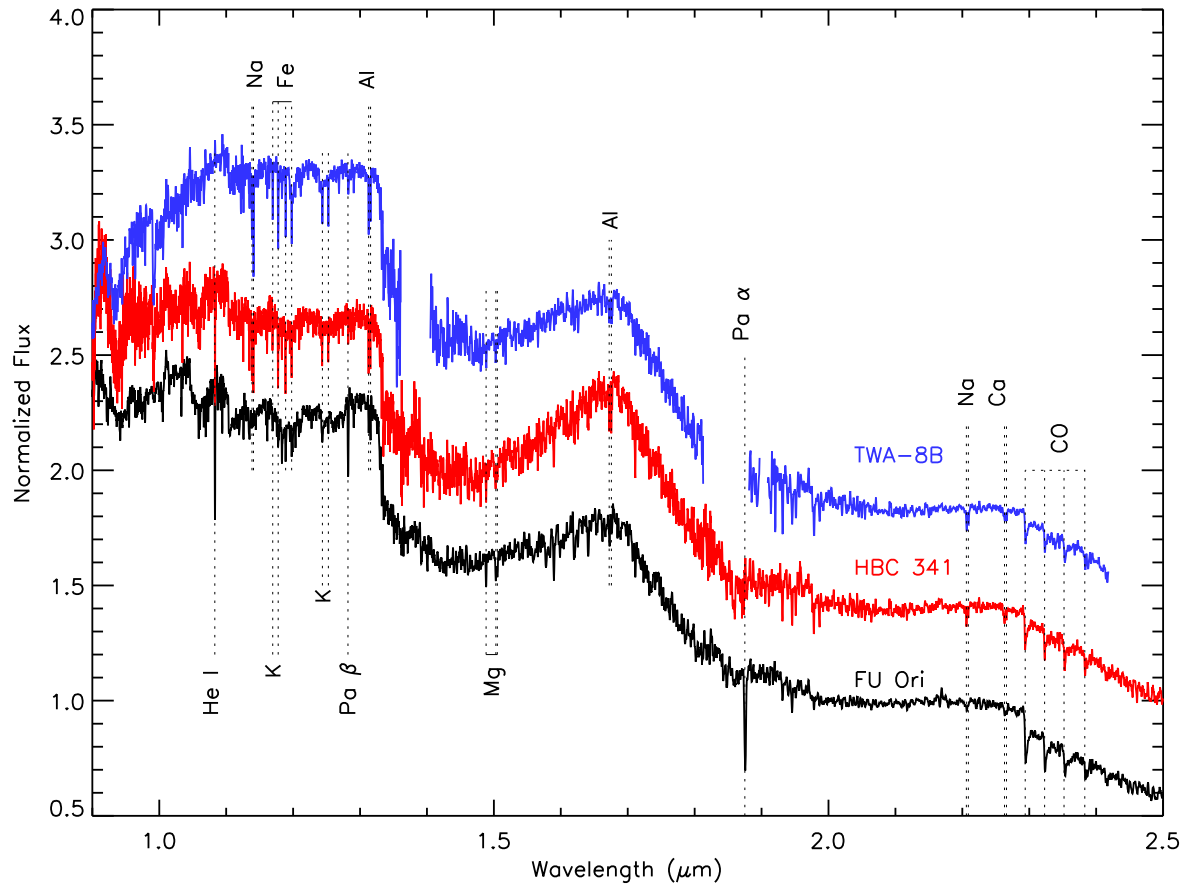


Fig. 12.— A comparison of the near-infrared spectrum of FU Ori with that of the newborn M5-type border-line brown dwarf HBC 341 (from Dahm & Hillenbrand 2017) and the 10 Myr old brown dwarf TWA-8B (from Allers & Liu 2013). Selected lines are identified.

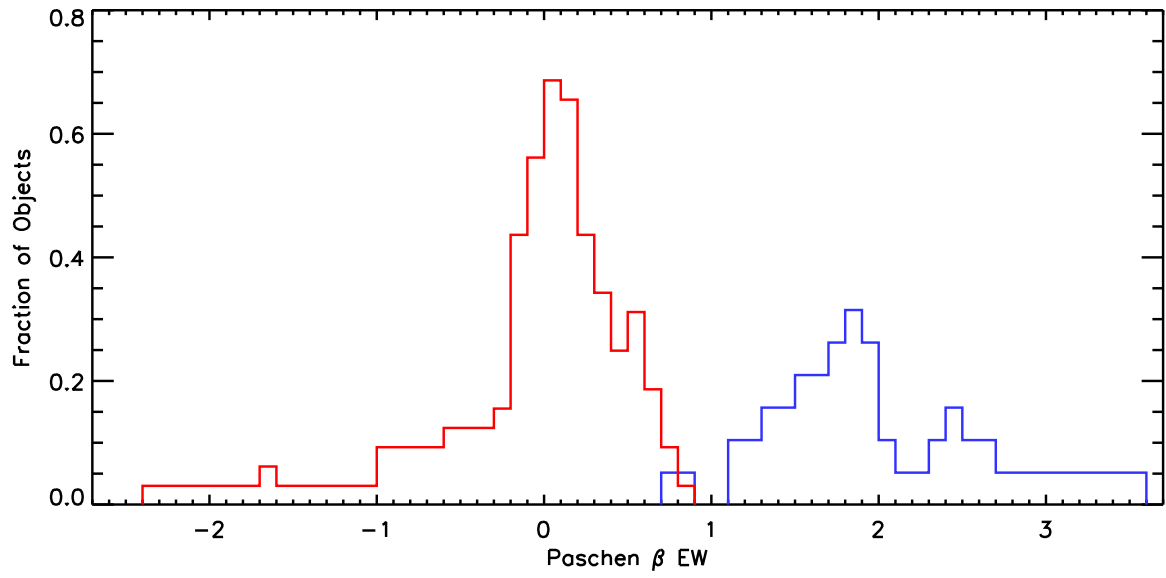


Fig. 13.— Distribution of equivalent widths of the Paschen- β line in young brown dwarfs (red, from Allers & Liu 2013) just overlaps with the distribution for FUors and FUor-like objects (blue, this paper), suggesting that Pa β is a useful spectroscopic discriminator between the two types of objects.

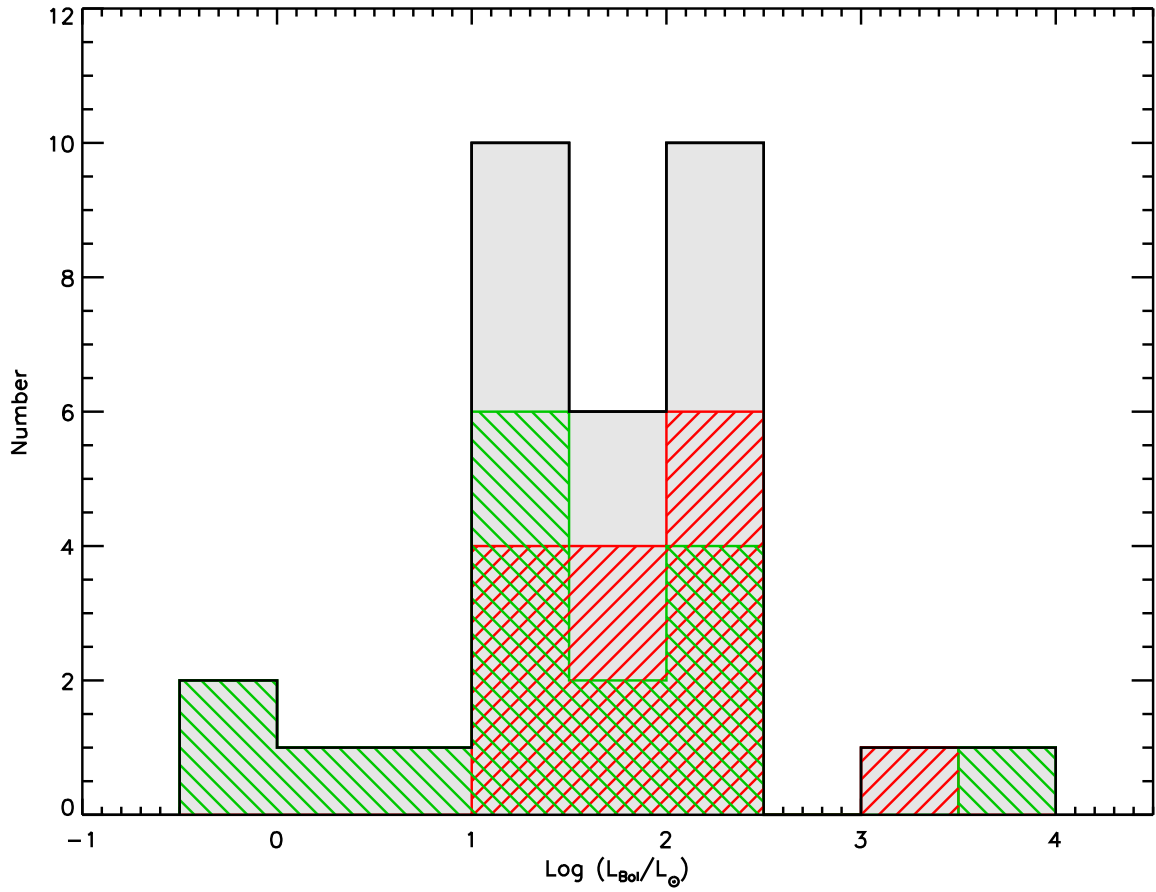


Fig. 14.— The bolometric luminosity distributions for the FUors (red), FUor-like objects (green), and the combined sample (black). Although the FUor-like objects have more low-luminosity objects, these two distributions are not significantly distinguishable.

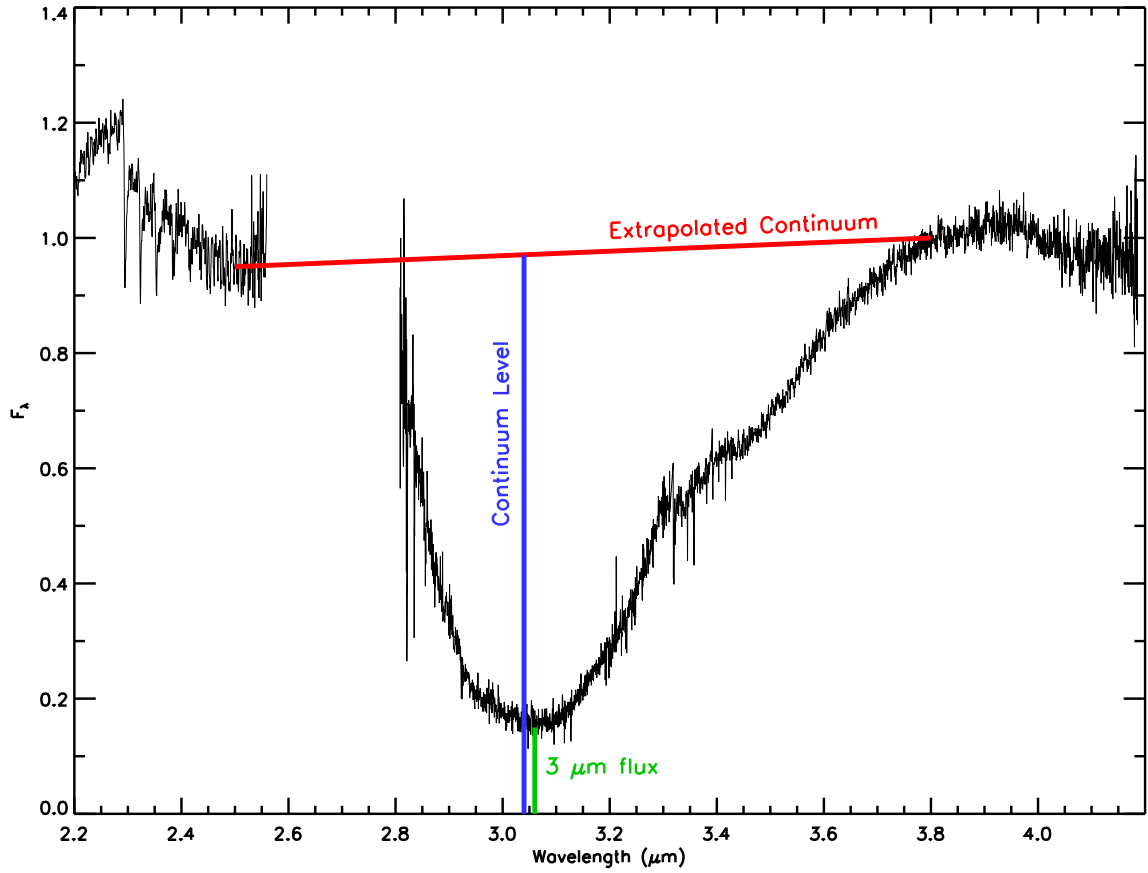


Fig. 15.— To measure the depth of the ice band, we first extrapolated the continuum from 2.5 to 3.8 μm . The relative ice band optical depth is calculated as $-\ln(\text{continuum level}/\text{flux at } 3 \mu\text{m})$.

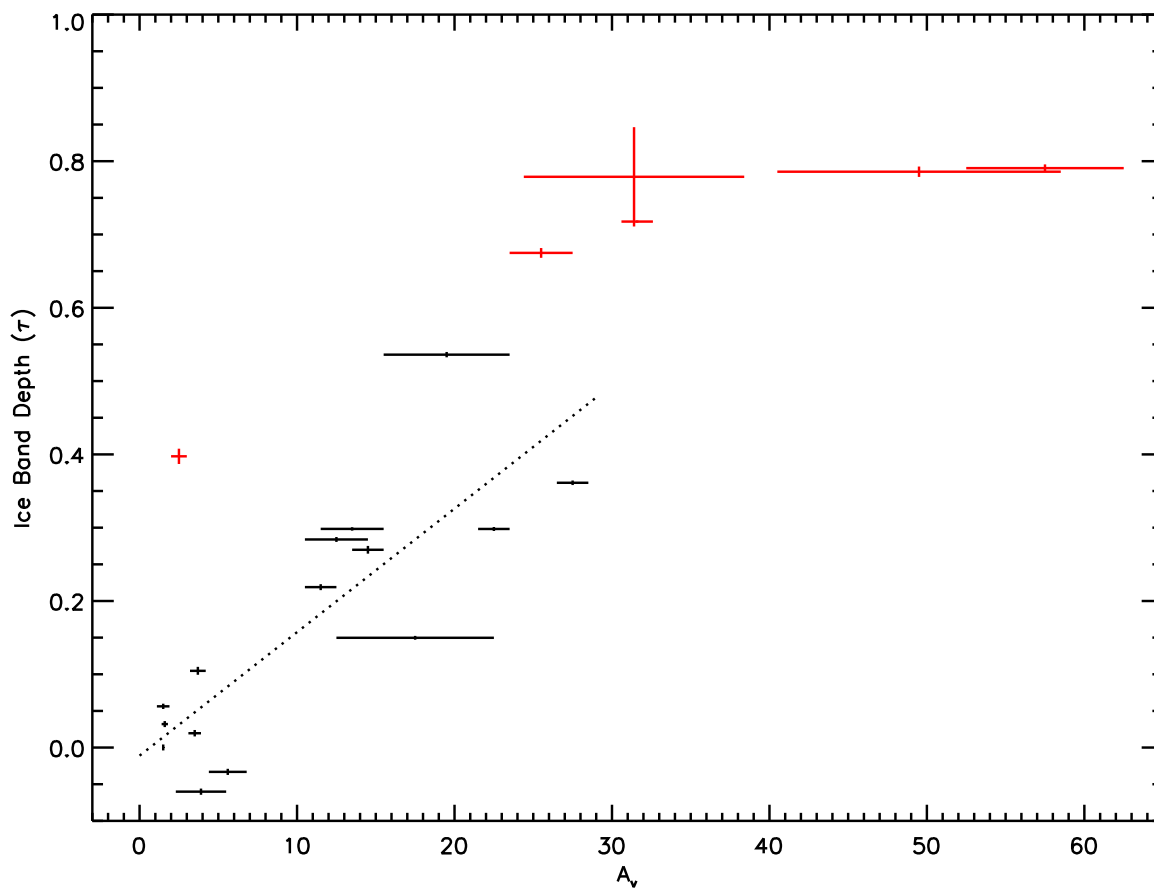


Fig. 16.— The $3.0 \mu\text{m}$ water ice absorption band optical depth (τ) is well correlated with the extinction for FUors, but there are a few notable exceptions. The black data points are objects not having a reflection nebula at K-band. The red data points are those objects with an infrared reflection nebula, and thus mostly seen in scattered light at K-band, which were also bright enough at L-band (Parsamian 21, L1551 IRS 5, HH354 IRS, IRAS 05450+0019, Haro 5a. and V2495 Cyg). The dotted line is our linear fit to the data except for the two objects with the highest extinction, as the optical depth appears to saturate when A_v exceeds ~ 30 . In most cases, the y-axis error bars are too small to be seen.

Table 1. Observing Log

| Name | Photometry | SXD | | LXD | |
|-------------------|-------------|-------------|------------------------|-------------|-----------|
| | | Date | Int. time ^a | Date | Int. time |
| RNO 1b | 28 Aug 2015 | 28 Aug 2015 | 18.0 | 28 Aug 2015 | 4.0 |
| RNO 1c | 28 Aug 2015 | 28 Aug 2015 | 12.0 | 28 Aug 2015 | 4.0 |
| PP 13 S | 21 Nov 2015 | 16 Jan 2015 | 12.0 | 31 Oct 2015 | 8.0 |
| L1551 IRS 5 | 21 Nov 2015 | 04 Nov 2015 | 24.0 | 28 Aug 2015 | 4.0 |
| V582 Aur | 30 Oct 2015 | 20 Jan 2015 | 8.0 | 30 Oct 2015 | 4.0 |
| Haro 5a/6a | 30 Oct 2015 | 30 Oct 2015 | 24.0 | 05 Jan 2016 | 16.0 |
| V883 Ori | 30 Oct 2015 | 30 Oct 2015 | 4.0 | 30 Oct 2015 | 1.2 |
| V2775 Ori | 30 Oct 2015 | 30 Oct 2015 | 16.0 | 04 Nov 2015 | 4.0 |
| FU Ori | 21 Nov 2015 | 08 Jan 2015 | 1.3 | 08 Jan 2015 | 2.7 |
| V1647 Ori | 21 Nov 2015 | 04 Nov 2015 | 18.0 | 04 Nov 2015 | 4.0 |
| NGC2071 MM3 | 21 Nov 2015 | 04 Nov 2015 | 24.0 | 04 Nov 2015 | 4.0 |
| IRAS 06297+1021W | 16 Nov 2006 | 16 Nov 2006 | 8.0 | | |
| AR 6a | 21 Nov 2015 | 04 Nov 2015 | 24.0 | 04 Nov 2015 | 4.0 |
| AR 6b | 21 Nov 2015 | 21 Nov 2015 | 36.0 | | |
| IRAS 06393+0913 | 15 Oct 2007 | 15 Oct 2007 | 30.0 | | |
| V900 Mon | 21 Nov 2015 | 20 Jan 2015 | 12.0 | 22 Jan 2015 | 5.3 |
| V960 Mon | 21 Dec 2014 | 19 Dec 2014 | 16.0 | 19 Dec 2014 | 5.3 |
| Z CMa | 21 Nov 2015 | 09 Jan 2015 | 1.6 | 09 Jan 2015 | 1.3 |
| BBW 76 | 21 Nov 2015 | 09 Jan 2015 | 8.0 | 09 Jan 2015 | 2.7 |
| V346 Nor | 22 Jul 2015 | 22 Jul 2015 | 36.0 | 22 Jul 2015 | 8.0 |
| IRAS 18270-0153 W | | 31 Aug 2015 | 24.0 | 31 Aug 2015 | 8.0 |
| V371 Ser | 18 Jul 2016 | 18 Jul 2016 | 264.0 ^b | | |
| IRAS 18341-0113 S | 26 Jun 2015 | 26 Jun 2015 | 36.0 | | |
| Parsamian 21 | 27 May 2016 | 31 Aug 2015 | 16.0 | 31 Aug 2015 | 8.0 |
| V1515 Cyg | 26 Jun 2015 | 26 Jun 2015 | 12.0 | 26 Jun 2015 | 5.3 |
| HBC 722 | 31 Oct 2015 | 31 Oct 2015 | 12.0 | 31 Oct 2015 | 4.0 |
| V2494 Cyg | 30 Oct 2015 | 30 Oct 2015 | 24.0 | 30 Oct 2015 | 4.0 |
| V1057 Cyg | 26 Jun 2015 | 26 Jun 2015 | 8.0 | 26 Jun 2015 | 2.7 |
| V2495 Cyg | 10 Dec 2015 | 27 May 2016 | 64.0 | 18 Jul 2016 | 20.0 |
| CB230 | 28 Aug 2015 | 28 Aug 2015 | 24.0 | 28 Aug 2015 | 2.7 |
| V1735 Cyg | 28 Aug 2015 | 28 Aug 2015 | 12.0 | 28 Aug 2015 | 2.7 |
| HH354 IRS | 30 Oct 2015 | 08 Jul 2016 | 72.0 ^b | 31 Oct 2015 | 8.0 |
| V733 Cep | 26 Jun 2015 | 26 Jun 2015 | 18.0 | 26 Jun 2015 | 8.0 |

^aThe integration times are given in minutes

^bObserved with the 0''.8 slit. All others were observed with the 0''.5 slit.

Table 2. Sample Characteristics

| Name | Alt. Name | α (J2000) ^a | δ (J2000) ^a | K ^b | Group ^c | Dist (pc) ^d | L_{bol} ^e | A_v ^f |
|-------------------|-----------------------------|-------------------------------|-------------------------------|--------------------|--------------------|------------------------|------------------------|--------------------|
| RNO 1b | V710 Cas | 00:36:46.3 | +63:28:54 | 8.34 | FUor | 930±35 (1) | 1652 | 14.5±1 |
| RNO 1c | V710 Cas | 00:36:46.4 | +63:28:55 | 7.73 | FUor-like | 930±35 (1) | 1652 | 19.5±4 |
| PP 13 S | IRAS 04073+3800 | 04:10:41.1 | +38:07:53 | 10.82 | FUor-like | 450±23 (2) | 51 | 56.5±5 |
| L1551 IRS 5 | IRAS 04287+1801 | 04:31:34.2 | +18:08:05 | 9.21 | FUor-like | 147±5 (3,4) | 29 | 25.5±2 |
| V582 Aur | | 05:25:52.0 | +34:52:30 | 8.18 | FUor | 1300 (5) | 168 | 5.6±1.2 |
| Haro 5a/6a | IRAS 05329-0505 | 05:35:26.6 | -05:03:56 | 9.85 | FUor-like | 388±5 (6) | 18 | 57.5±5 |
| V883 Ori | HBC 489 | 05:38:18.1 | -07:02:26 | 5.53 | FUor | 388±5 (6) | 212 | 22.5±1 |
| V2775 Ori | HOPS 223 | 05:42:48.5 | -08:16:35 | 8.43 | FUor | 428±10 (6) | 29 | 27.5±1 |
| FU Ori | IRAS 05426+0903 | 05:45:22.4 | +09:04:12 | 5.79 | FUor | 400±40 (7) | 66 | 1.5±0.2 |
| V1647 Ori | McNeil’s Nebula | 05:46:13.1 | -00:06:05 | 7.90 | Peculiar | 388±5 (6) | 21 | 22.5±7 |
| IRAS 05450+0019 | NGC2071 MM3 | 05:47:36.6 | +00:20:06 | 8.76 | FUor-like | 388±5 (6) | 35 | 31.5±1 |
| IRAS 06297+1021W | | 06:32:26.1 | +10:19:18 | 8.14 | Peculiar | 738±57 (8) | 31 | 10.3±3.8 |
| AR 6a | V912 Mon | 06:40:59.3 | +09:35:52 | 7.88 | Peculiar | 738±57 (8) | 310 | 20.5±2 |
| AR 6b | | 06:40:59.3 | +09:35:52 | 10.89 | Peculiar | 738±57 (8) | 310 | 28.5±3 |
| IRAS 06393+0913 | | 06:42:08.1 | +09:10:30 | 10.45 | Peculiar | 738±57 (8) | 0.9 | 23.5±7 |
| V900 Mon | | 06:57:22.2 | -08:23:18 | 7.51 | FUor | 1100 (9) | 99 | 13.5±2 |
| V960 Mon | | 06:59:31.6 | -04:05:28 | 7.42 | FUor | 1100 (9) | 48 | 1.5±0.4 |
| Z CMa | HD 53179 | 07:03:43.2 | -11:33:06 | 3.77 ^b | FUor-like | 990±50 (10) | 3548 | 7.1±8.0 |
| BBW 76 | V646 Pup | 07:50:35.6 | -33:06:24 | 8.60 | FUor-like | 1800 (11) | 114 | 1.6±0.2 |
| V346 Nor | HH57 IRS | 16:32:32.1 | -44:55:31 | 10.51 | Peculiar | 700 (12) | 176 | 46.5±9 |
| IRAS 18270-0153 W | | 18:29:38.9 | -01:51:06 | 12.87 ^b | Peculiar | 436±9 (13) | 30 | 41.5±11 |
| V371 Ser | EC 53 | 18:29:51.2 | +01:16:39 | 12.19 | Peculiar | 429±2 (14) | 1.6 | 47.5±9 |
| IRAS 18341-0113 S | | 18:36:46.5 | -01:10:42 | 11.39 | Peculiar | 259±37 (15) | 0.8 | 31.5±6 |
| Parsamian 21 | IRAS 19266+0932, HBC 687 | 19:29:00.8 | +09:38:43 | 9.55 | FUor-like | 500 (16) | 16 | 2.5±0.5 |
| V1515 Cyg | IRAS 20220+4202 | 20:23:48.0 | +42:12:26 | 7.95 | FUor | 1050 (17) | 103 | 3.5±0.4 |
| HBC 722 | V2493 Cyg | 20:58:17.0 | +43:53:43 | 6.31 | FUor | 550±50 (18) | 17 | 3.7±0.5 |
| V2494 Cyg | IRAS 20568+5217, HH381 IRS | 20:58:21.4 | +52:29:27 | 8.37 | FUor | 600 (19) | 187 | 17.5±5 |
| V1057 Cyg | LkH α 190 | 20:58:53.7 | +44:15:29 | 6.59 | FUor | 550±50 (18) | 100 | 3.9±1.6 |
| V2495 Cyg | Braid star | 21:00:25.4 | +52:30:16 | 11.79 | FUor | 600 (19) | 21 | 49.5±9 |
| CB230 | IRAS 21169+6804 | 21:17:39.4 | +68:17:32 | 10.27 | FUor-like | 300±30 (20) | 6.6 | 26.5±7 |
| V1735 Cyg | IRAS 21454+4718, HBC 733 | 21:47:20.7 | +47:32:04 | 7.54 | FUor | 950±80 (21) | 166 | 12.5±2 |
| HH354 IRS | IRAS 22051+5848, L1165 IRS1 | 22:06:50.2 | +59:02:45 | 10.83 | FUor-like | 300±100 (22) | 16 | 31.5±7 |
| V733 Cep | Persson’s Star | 22:53:33.3 | +62:32:24 | 8.29 | FUor | 800 (23) | 43 | 11.5±1 |

^a2MASS coordinate for the target

^bK-band magnitudes from our observations, and are in the MKO photometric system unless otherwise noted. Z CMa was observed through the narrow K-continuum filter to avoid saturation. 2MASS photometry is given for IRAS 18270-0153 #7.

^cFUor: Eruption observed; FUor-like: Eruption not observed, but spectrum similar to FUors; Peculiar: Has some spectroscopic or photometric similarities to FUors

^d(1) Reid et al. 2014 (2) Lada et al. 2009 (3) Loinard et al. 2007 (4) This paper (5) Kun et al. 2017 (6) Kounkel et al. 2017 (7) Murdin & Penston 1977 (8) Kamezaki et al. 2014 (9) Kim et al. 2004 (10) Kaltcheva & Hilditch 2000 (11) Reipurth et al. 2002 (12) Graham & Frogel 1985 (13) Ortiz-León et al. 2016 (14) Dzib et al. 2011 (15) Straizys et al. 1996 (16) Dame & Thaddeus 1985 (17) Racine 1968 (18) Laugalys et al. 2006 (19) Herbig & Dahm 2006 (20) Kun et al. 1998 (21) Harvey et al. 2008 (22) Dobashi et al. 1994 (23) Reipurth et al. 2007

^eThe bolometric luminosity was calculated using photometry from 2MASS (1.2 to 2.2 μ m), WISE (3.4 to 22 μ m), and Akari (65 to 160 μ m). An 80 K black body was added to reddest data point. For RNO 1b/c and AR 6a/b the binary was not resolved.

^fVisual extinction in magnitudes, derived from fitting the spectrum to FU Ori and adding FU Ori’s 1.5 magnitudes of extinction.

Table 3. Basis of FUor Classification

| Name | Eruption Observed? | CO abs. | Water abs. | VO or ^a TiO | Pa β abs. | Emission Lines | weak metals | He I abs. |
|------------------------|-----------------------|------------|---------------|---------------------------|--------------------|-------------------|----------------|--------------|
| Bona fide FUors | | | | | | | | |
| RNO 1b | Y | Y | Y | Y | Y | N | Y | Y |
| V582 Aur | Y | Y | Y | Y | Y | N | Y | Y |
| V883 Ori | Y | Y | Y | Y | Y | N | Y | N |
| V2775 Ori | Y | Y | Y | Y | Y | N | Y | Y |
| FU Ori | Y | Y | Y | Y | Y | N | Y | Y |
| V900 Mon | Y | Y | Y | Y | Y | N | Y | Y |
| V960 Mon | Y | Y | Y | Y | Y | N | Y | Y |
| V1515 Cyg | Y | Y | Y | Y | Y | N | Y | Y |
| HBC 722 | Y | Y | Y | Y | Y | N | Y | Y |
| V2494 Cyg | Y | Y | Y | Y | Y | Y | Y | Y |
| V1057 Cyg | Y | Y | Y | Y | Y | N | Y | Y |
| V2495 Cyg | Y | Y | Y | no data | no data | N | Y | no data |
| V1735 Cyg | Y | Y | Y | Y | Y | N | Y | Y |
| V733 Cep | Y | Y | Y | Y | Y | N | Y | N |
| FUor-like | | | | | | | | |
| RNO 1c | N | Y | N | N | Y | N | Y | N |
| PP 13 S | N | Y | Y | no data | no data | Y | Y | no data |
| L1551 IRS 5 | N | Y | Y | Y | N | Y | Y | N |
| Haro 5a/6a | N | Y | Y | no data | no data | N | Y | no data |
| IRAS 05450+0019 | N | Y | Y | no data | N | N | Y | no data |
| Z CMa | N | N | N | N | N | Y | Y | Y |
| BBW 76 | N | Y | Y | Y | Y | N | Y | Y |
| Parsamian 21 | N | Y | Y | Y | Y | N | Y | Y |
| CB230 IRS1 | N | Y | Y | no data | no data | Y | Y | no data |
| HH354 IRS | N | Y | Y | no data | no data | N | Y | no data |
| Peculiar | | | | | | | | |
| V1647 Ori | Y | N | Y | Y | N | Y | Y | Y |
| IRAS 06297+1021W | N | N | Y | N | N | Y | Y | Y |
| AR 6a | N | N | N | N | Y | N | Y | Y |
| AR 6b | N | Y | N | no data | N | N | Y | no data |
| IRAS 06393+0913 | N | Y | N | N | N | N | Y | no data |
| V346 Nor | Y | N | N | no data | no data | Y | Y | no data |
| V371 Ser | N | Y | Y | no data | no data | Y | Y | no data |
| IRAS 18270-0153W | N | N | Y | no data | no data | Y | Y | no data |
| IRAS 18341-0113S | N | N | Y | no data | no data | Y | Y | no data |

^aSee Figure 1 or location of VO and TiO absorption bands